IMMUNOLOGY

Gut IgA functionally interacts with systemic IgG to enhance antipneumococcal vaccine responses

Cindy Gutzeit[1]†‡, Emilie K. Grasset[2,3,4]*†, Dean B. Matthews[5,6]§, Paul J. Maglione[7]§, Graham J. Britton[8], Haley Miller[1], Giuliana Magri[9]¶, Lewis Tomalin[10], Matthew Stapylton[10], Pablo Canales-Herrerias[1], Musia Sominskaia[2], Mauricio Guzman[9], Marc Pybus[11], Sonia Tejedor Vaquero[9], Lin Radigan[12], Roser Tachó-Piñot[9], Andrea Martín Nalda[13,14,15], Marina García Prat[13,14,15], Monica Martinez Gallo[14,16], Romina Dieli-Crimi[16], José C. Clemente[1,10], Saurabh Mehandru[1,17], Mayte Suarez-Farinas[10], Jeremiah J. Faith[1,10], Charlotte Cunningham-Rundles[12], Andrea Cerutti[1,9,18]*

The gut microbiota enhances systemic immunoglobulin G (IgG) responses to vaccines, but it is unknown whether this effect involves IgA, which coats intestinal microbes. That IgA may amplify postimmune IgG production is suggested by the impaired IgG response to pneumococcal vaccines in some IgA-deficient patients. Here, we found that antipneumococcal but not total IgG production was impaired in mice with IgA deficiency. The positive effect of gut IgA on antipneumococcal IgG responses started very early in life and could implicate gut bacteria, as these responses were attenuated in germ-free mice recolonized with gut microbes from IgA-deficient donors. IgA could exert this effect by constraining the systemic translocation of gut antigens, which was associated with chronic immune activation, including T cell overexpression of programmed cell death protein 1 (PD-1). This inhibitory receptor may attenuate antipneumococcal IgG production by causing B cell hyporesponsiveness, which improved upon anti–PD-1 treatment. Thus, gut IgA functionally interacts with systemic IgG to enhance antipneumococcal vaccine responses.

INTRODUCTION

The intestinal mucosa includes commensal bacteria, fungi, viruses, and other microbial and eukaryotic species collectively referred to as microbiota, which modulates host immunity, including immune responses to vaccines (*1*, *2*). While most of these studies have focused on the microbial component of the gut microbiota, this "prokaryotic organ" of our body also includes immunoglobulin A (IgA), a prominent mucosal antibody from intestinal B cells that coats commensal microbes (*3*). Yet, the role of gut IgA in systemic immunity remains unclear.

IgA mostly derives from intestinal B cell responses to commensal bacteria, which function as major IgA inducers (*3*). These responses occur under homeostatic conditions through complementary T cell–dependent (TD) and T cell–independent (TI) pathways that yield distinct pools of IgA antibodies, at least in mice (*4*, *5*). Conversely, IgA interaction with gut commensals shapes the topography, composition, and immunometabolic properties of the intestinal microbiota (*6*). However, the impact of gut IgA on systemic IgG responses remains elusive.

Growing evidence indicates that IgA cooperates with IgG to enhance protection against both commensals and pathogens (*7*, *8*). Accordingly, some patients with IgA deficiency (IGAD) develop mucosal infections, including respiratory infections, in addition to gut dysbiosis (*9*, *10*). Of note, infections by common lung pathogens such as *Streptococcus pneumoniae* are usually controlled by IgG, which can be readily elicited by pneumococcal vaccines (*11*). Some patients with IGAD and with heterogeneous phenotypic traits show impaired systemic IgG responses to pneumococcal vaccines (*12*, *13*). In addition, some patients with IGAD exhibit a concomitant IgG subclass deficiency, whereas others develop a global and profound IgG depletion as they progress to common variable immunodeficiency (*14*). Together, these observations suggest that IgA may be more functionally connected to IgG than commonly thought.

Accordingly, the IgA-targeted motility protein flagellin from gut microbes enhances IgG responses to an influenza vaccine in addition to promoting IgA production (*15*, *16*). Similarly, gut microbial

[1]Department of Medicine, Precision Immunology Institute, Icahn School of Medicine at Mount Sinai, New York, NY 10029, USA. [2]Department of Pediatrics, Weill Cornell Medicine, New York, NY 10021, USA. [3]Gale and Ira Drukier Institute for Children's Health, Weill Cornell Medicine, New York, NY 10021, USA. [4]Department of Microbiology and Immunology, Weill Cornell Medicine, New York, NY 10065, USA. [5]Immunology Program of the Sloan Kettering Institute, Memorial Sloan Kettering Cancer Center, New York, NY 10065, USA. [6]Immunology and Microbial Pathogenesis Program, Weill Cornell Graduate School of Medical Sciences, New York, NY 10065, USA. [7]Pulmonary Center and Department of Medicine, Boston University, Boston, MA 02118, USA. [8]Precision Immunology Institute, Icahn Institute for Data Science and Genome Technology, School of Medicine at Mount Sinai, New York, NY 10029, USA. [9]Program for Inflammatory and Cardiovascular Disorders, Institute Hospital del Mar for Medical Investigations (IMIM), 08003 Barcelona, Spain. [10]Department of Genetics and Genomic Sciences, Icahn Institute for Genomics and Multiscale Biology, Icahn School of Medicine at Mount Sinai, New York, NY 10029, USA. [11]Molecular Biology Laboratory, Fundació Puigvert, Instituto de Investigaciones Biomédicas Sant Pau (IIB-Sant Pau), 02041 Barcelona, Spain. [12]Departments of Medicine and Pediatrics, Precision Immunology Institute, Icahn School of Medicine at Mount Sinai, New York, NY 10029, USA. [13]Infection in Immunocompromised Pediatric Patients Research Group, Vall d'Hebron Institut de Recerca (VHIR), Vall d'Hebron University Hospital (HUVH), Vall d'Hebron Barcelona Hospital Campus, 08035 Barcelona, Spain. [14]Pediatric Infectious Diseases and Immunodeficiencies Unit, Vall d'Hebron University Hospital (HUVH), Barcelona Autònoma University (UAB), 48201 Barcelona, Spain. [15]Jeffrey Modell Diagnostic and Research Center for Primary Immunodeficiencies, 08035 Barcelona, Spain. [16]Division of Immunology, Vall d'Hebron University Hospital (HUVH), Barcelona Autònoma University (UAB), 48201 Barcelona, Spain. [17]Division of Gastroenterology, Precision Immunology Institute, Icahn School of Medicine at Mount Sinai, New York, NY 10029, USA. [18]Catalan Institute for Research and Advanced Studies (ICREA), 08003 Barcelona, Spain.
*Corresponding author. Email: emg4011@med.cornell.edu (E.K.G.); acerutti@imim.es (A.C.)
†These authors contributed equally to this work.
‡Present address: GSK, Rixensart, Belgium.
§These authors contributed equally to this work.
¶Present address: Immunology Unit, Department of Biomedical Sciences, Faculty of Medicine and Health Sciences, University of Barcelona, Barcelona, Spain.

metabolites amplify IgG in addition to IgA responses (*17*). Conversely, immune adaptations to the microbiota, including homeostatic IgA production, limit the potentially harmful host tissue response caused by unrestrained penetration of gut metabolites into tissues (*18*). This response usually entails a proinflammatory switch to IgG (*19*). Notwithstanding this evidence, whether intestinal IgA influences systemic IgG production remains unknown.

Here, we report that peripheral IgG responses to pneumococcal vaccines were compromised in IgA-deficient *Igha*$^{-/-}$ mice. This impairment was associated with increased systemic penetration of gut antigens and could be partly recapitulated in ex-germfree (GF) recipient mice recolonized with gut microbes from *Igha*$^{-/-}$ donors. Impaired postimmune IgG responses were associated with increased immune activation, including grossly augmented preimmune IgG production, some of which targeted gut commensal antigens. Increased immune activation further encompassed enhanced germinal center (GC) and plasma cell (PC) differentiation as well as augmented T cell expression of the immune inhibitor programmed cell death protein 1 (PD-1). Of note, PD-1 may contribute to the weakening of postimmune IgG production, which ameliorated upon anti–PD-1 treatment. Last, IgG responses were already perturbed in *Igha*$^{-/-}$ mice soon after birth. Together, our data unveil a hitherto unknown functional interconnection between gut IgA and systemic IgG responses.

RESULTS

IgA augments IgG responses to TD immunogens

Microbial carbohydrates with repetitive structure, including pneumococcal polysaccharides (PPS), induce specific IgM as well as IgG responses by activating splenic marginal zone (MZ) B cells in a TI manner, as opposed to microbial proteins that activate follicular (FO) B cells in a TD manner (*11*, *20*). The human vaccine Pneumovax23, which includes unconjugated PPS from 23 highly pathogenic serotypes of *S. pneumoniae*, induces humoral protection in adults but not young individuals due to the incomplete development of the splenic MZ in the first 5 years of life (*21*, *22*). To compensate for this limitation, the protein-conjugated pneumococcal vaccine Prevnar13, which encompasses protein-conjugated PPS from 13 highly pathogenic serotypes of *S. pneumoniae*, was developed. By eliciting specific IgG responses in a TD manner, Prevnar13 generates immune protection not only in children but also in adults unresponsive to Pneumovax23, which is a weaker immunogen (*21*, *22*).

First, we determined whether IGAD impaired systemic IgG responses to Prevnar13 in IgA-deficient C57BL/6 *Igha*$^{-/-}$ mice. These mice were generated by deleting the following genetic elements from the mouse Ig heavy chain (IgH) locus: (i) the Iα exon, which initiates germline transcription of both switch α region and constant α gene; (ii) the intronic switch α region, which guides class switching from IgM to IgA; and (iii) the 5′ half of the constant α gene, which encodes the constant α region of IgA (*23*). Wild-type (WT) and *Igha*$^{-/-}$ strains were generated by mating heterozygous *Igha*$^{+/-}$ parents to control for microbiota and genetic background variability between strains. WT mice used came from these strains, unless indicated otherwise.

Enzyme-linked immunosorbent assay (ELISA) showed that, compared to WT controls, *Igha*$^{-/-}$ mice induced less IgG1 to PPS from the Prevnar13 vaccine 7 and 28 days following intravenous immunization (Fig. 1A). Of note, this decrease was not associated with gross quantitative alterations of splenic IgG1 class–switched B cells (SBCs), plasmablasts, or PCs (Fig. 1B and fig. S1A). We then verified whether IGAD impaired the magnitude and affinity of systemic IgG1 responses to 4-hydroxy-3-nitrophenyl-ovalbumin (NP-OVA), a commonly used TD immunogen. Compared to WT controls, *Igha*$^{-/-}$ mice induced less IgG1 with either high (NP7) or low (NP23) affinity 7, 14, 21, 28, and 62 days following intraperitoneal immunization with NP-OVA and aluminum hydroxide and magnesium hydroxide (alum) (Fig. 1C and fig. S1B). In immunized *Igha*$^{-/-}$ mice, the reduction of IgG1 affinity maturation was most evident at days 7 and 14 and remained significant up to day 28 (Fig. 1D).

We therefore wondered whether IGAD depleted FO B cell precursors of TD IgG1-secreting cells and found that the absolute number but not the frequency of these cells was increased in *Igha*$^{-/-}$ mice compared to WT controls (Fig. 1, E and F). We further evaluated whether IGAD caused B cell–intrinsic alterations of TD-induced IgG1 class switching and secretion. Splenic B cells from *Igha*$^{-/-}$ mice induced surface IgG1 expression, PC differentiation, and IgG1 secretion as much as splenic B cells from WT controls upon incubation for 6 days with an agonistic antibody to CD40 mimicking CD40 ligand and interleukin-4 (IL-4) (Fig. 1, G to K).

Last, we determined whether IGAD altered splenic T cells and dendritic cells (DCs), which are essential for FO B cells to initiate TD antibody responses (*21*). Compared to WT controls, *Igha*$^{-/-}$ mice showed overlapping frequencies and absolute numbers of total T cells as well as $CD4^+$, $CD8^+$, or $CD4^-CD8^-$ T cell subsets, except that the frequency of $CD4^-CD8^-$ T cells was slightly decreased and the absolute number of $CD4^+$ T cells was slightly increased (fig. S1C). Compared to WT controls, *Igha*$^{-/-}$ mice also showed overlapping frequencies and absolute numbers of total DCs as well as $CD4^+CD8^-$, $CD4^-CD8^+$, or $CD4^-CD8^-$ DC subsets (fig. S1D). Thus, IgA may enhance systemic IgG responses to TD immunogens through a B cell–extrinsic mechanism that could operate upstream of PC differentiation.

IgA enhances IgG responses to TI immunogens

Next, we determined systemic IgG responses to Pneumovax23 in *Igha*$^{-/-}$ mice. Compared to WT controls, *Igha*$^{-/-}$ mice did not induce plasma IgG3 to PPS at 3 and 7 days following intravenous immunization with Pneumovax23 (fig. S2A). Together with IgG3, IgM is a major component of humoral immunity to TI antigens (*20*), and *Igha*$^{-/-}$ mice produced more PPS-specific IgM both at baseline and after Pneumovax23 immunization compared to WT controls (fig. S2A). Like Pneumovax23, replication-incompetent *S. pneumoniae* induced less specific IgG3 but more specific IgM in *Igha*$^{-/-}$ mice at day 7 following intravenous immunization (fig. S2B).

Then, we ascertained whether IGAD impaired IgG3 responses to TI antigens other than unconjugated PPS. Compared to WT controls, *Igha*$^{-/-}$ mice showed no 2,4,6-trinitrophenyl (TNP)–specific IgG3 but increased TNP-specific IgM at steady state and 3 and 5 days following intravenous immunization with TNP-Ficoll (fig. S2C), a haptenated polysaccharide structurally mimicking native PPS. While TNP-Ficoll activates MZ and B-1 B cells by cross-linking the B cell antigen receptor (BCR), TNP–lipopolysaccharide (LPS) activates MZ and B-1 B cells by coengaging Toll-like receptor 4 and BCR (*24*). Compared to WT controls, *Igha*$^{-/-}$ mice induced less TNP-specific IgG3 but more TNP-specific IgM 3 and 7 days following intravenous immunization with TNP-LPS (fig. S2D). We therefore wondered whether IGAD globally impaired IgG3 production. Total plasma IgG3 was readily detectable in *Igha*$^{-/-}$ mice, although less compared

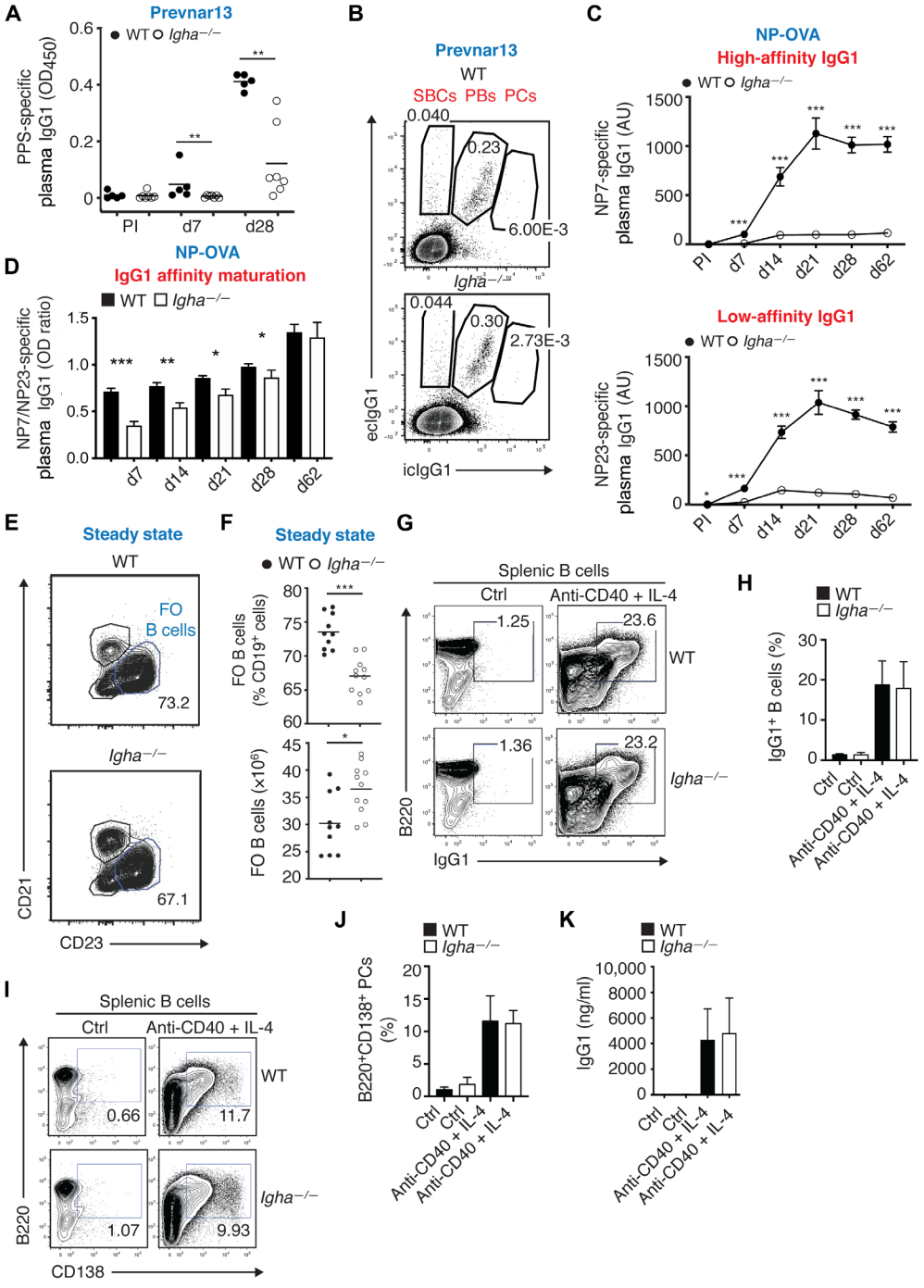

Fig. 1. IgA increases systemic IgG responses to TD immunogens, including protein-conjugated pneumococcal vaccine. (**A**) ELISA of plasma IgG1 to PPS from five WT or seven *Igha*$^{-/-}$ mice prior to immunization (PI) and following Prevnar13 intravenously. (**B**) Flow cytometry of intracellular (ic) and extracellular (ec) IgG1 from splenic ecIgG1^{+}icIgG1^{-} SBCs, ecIgG1^{+}icIgG1^{+} plasmablasts (PBs), and ecIgG1^{lo}icIgG1^{+} PCs of representative WT or *Igha*$^{-/-}$ mice 28 days following Prevnar13 intravenously. Numbers indicate frequency of B220^{+} cells. (**C**) ELISA of plasma high- [NP7–bovine serum albumin (BSA)] and low-affinity (NP23-BSA) IgG1 and (**D**) IgG1 affinity maturation calculated as optical density (OD) ratio of high- and low-affinity IgG1 in 13 WT or 11 *Igha*$^{-/-}$ mice following NP15-OVA and aluminum hydroxide and magnesium hydroxide (alum) intraperitoneally. (**E** and **F**) Steady-state flow cytometry of CD21^{low}CD23^{high} splenic FO B cells from representative WT or *Igha*$^{-/-}$ mice (E), frequency of CD19^{+} cells, and absolute number from 10 WT or 11 *Igha*$^{-/-}$ mice (F). (**G** and **H**) Flow cytometry of IgG1^{+}B220^{+} cells from splenic B cells of representative WT or *Igha*$^{-/-}$ mice incubated with medium alone (ctrl) or anti-CD40 and IL-4 for 6 days (G) and frequency of live cells from 6 WT or *Igha*$^{-/-}$ mice (H). (**I** and **J**) Flow cytometry of B220^{+}CD138^{+} PCs from splenic B cells of representative WT or *Igha*$^{-/-}$ mice incubated as in (G) (I) and frequency of live cells (J). (**K**) IgG1 ELISA from four WT or *Igha*$^{-/-}$ mice incubated as in (G). Data show representative mice [(B), (E), (G), and (I)], are representative of two experiments (F), or summarize results from either two [(A), (C), (D), and (K)] or three experiments [(H) and (J)]. Results are shown with mean [(A) and (F)] or mean ± SEM [(C), (D), (H), (J), and (K)]; two-tailed unpaired Student's *t* test used for normally distributed data otherwise Mann-Whitney test. *$P < 0.05$, **$P < 0.01$, and ***$P < 0.001$. d7, day 7; AU, arbitrary units.

to WT controls (fig. S2E). This finding ruled out a global impairment of IgM-to-IgG3 class switching and IgG3 secretion in B cells from *Igha*$^{-/-}$ mice. As reported earlier (*23*), these mice also showed more total plasma IgM compared to WT controls (fig. S2E), which implied that IGAD was not associated with a general impairment of B cell activation.

We next wondered whether IGAD caused MZ B cell depletion (*20*), but flow cytometry showed more splenic MZ B cells in *Igha*$^{-/-}$ mice compared to WT controls (fig. S2, F and G). We also determined whether IGAD impaired IgG3 class switching and PC differentiation in response to commonly used TI antigens. Compared to WT controls, splenic IgG3 class SBCs increased 5 days following intravenous immunization of *Igha*$^{-/-}$ mice with TNP-Ficoll, whereas IgG3 class–switched plasmablasts and PCs decreased (fig. S2, H and I). This decrease was not due to an intrinsic B cell defect, as splenic B cells from WT and *Igha*$^{-/-}$ mice cultured with the TI antigen LPS for 4 days comparably differentiated to plasmablasts (fig. S2, J and K). Thus, IgA enhances systemic IgG responses to TI immunogens through a B cell extrinsic mechanism involving PC differentiation and/or survival.

IgA restrains IgG responses to gut commensal antigens

Given the severe impairment of Prevnar13-induced IgG1 in *Igha*$^{-/-}$ mice, we next evaluated the effect of IgA on steady-state IgG1 production. Our choice of focusing hereafter on Prevnar13 and IgG1 was based on the following considerations. First, new clinical guidance recommends always using TD protein–conjugated Prevnar as clinical immunization practice (*25*). Second, IgG1 is increased in patients with IGAD, and this increase is associated with a biased T helper type 2 (T_H2) response, which drives strong IgG1-inducing signals to B cells (*26*). Third, as we have shown earlier, the IgG1 response to Prevnar13 is grossly impaired in *Igha*$^{-/-}$ mice. Fourth, aside from IgA, IgG1 is involved in anticommensal immunity (*27*), which may be altered in *Igha*$^{-/-}$ mice as is the case in patients with IGAD (*26*).

Consistent with an earlier study (*23*), we found that total plasma IgG1 was increased in *Igha*$^{-/-}$ mice compared to WT controls (Fig. 2A), which demonstrated that IgG1 production was not globally impaired in *Igha*$^{-/-}$ mice. Considering that IgA limits the penetration of gut commensal bacteria (*3*), we also ascertained whether IGAD increased the systemic IgG1 response to soluble microbial antigens. Compared to WT controls, *Igha*$^{-/-}$ mice showed more plasma IgG1 to lipoteichoic acid (LTA) from *Staphylococcus aureus*, capsular polysaccharide 14 (CPS14) from *S. pneumoniae*, LPS from *Salmonella typhimurium* as well as CPS9 from *S. pneumoniae* (Fig. 2B and fig. S3A).

We further determined whether IGAD increased peripheral IgG1 responses to gut microbiota antigens. ELISA showed that, compared to WT controls, *Igha*$^{-/-}$ mice had increased plasma IgG1 and IgM to gut bacteria from both small intestine (SI) and colon (Fig. 2, C and D, and fig. S3, B and C). The increased plasma IgG1 in *Igha*$^{-/-}$ mice reacted to total antigens (Fig. 2, C and D) and surface only antigens from whole bacteria (fig. S3B). Last, we explored gut IgG1 and IgM responses. Similar to an earlier study (*23*), *Igha*$^{-/-}$ mice showed increased total IgG1 and IgM in feces from both SI and colon compared to WT controls (fig. S3, D and E). Given that gut IgG usually increases as a result of inflammation (*19*, *28*), we microscopically analyzed the intestinal mucosa from *Igha*$^{-/-}$ mice, which was found to be histologically normal (fig. S3F and table S1).

Having shown that IGAD abnormally increased IgG1 production to gut commensal antigens, we evaluated whether this finding stemmed from augmented bacterial breaching of the intestinal barrier. Similar to mesenteric adipose tissue (MAT) from patients with Crohn's disease (*29*), MAT but not mesenteric lymph nodes (MLNs), liver, or spleen from *Igha*$^{-/-}$ mice yielded more colony-forming units (CFUs) upon incubation on agar plates placed in an anaerobic chamber compared to WT controls (Fig. 2E and fig. S3G). In keeping with an earlier study showing IgA-coated *Lactobacillus* (*30*), mass spectrometry showed increased *Lactobacillus*, including *Lactobacillus murinus*, *Lactobacillus reuteri*, and *Lactobacillus intestinalis*, in the MAT from *Igha*$^{-/-}$ mice (Fig. 2F and fig. S3H). Consistent with the possibility that IGAD enhances the systemic penetration of gut commensal antigens, quantitative polymerase chain reaction (PCR) detected an increased proportion of 16*S* bacterial DNA in the liver from *Igha*$^{-/-}$ mice, although this increase did not reach statistical significance (fig. S3I). Bacterial DNA was comparable in the spleen or MLNs from *Igha*$^{-/-}$ and WT mice (fig. S3I).

At variance with an earlier study showing no consistent microbiota changes in *Igha*$^{-/-}$ mice bred from *Igha*$^{+/-}$ parents (*31*), we detected some microbiota differences in these mice when studied through stool 16*S* ribosomal RNA (rRNA) gene sequencing (Fig. 2G). Compared to control *Igha*$^{+/+}$ littermates, cohoused *Igha*$^{-/-}$ mice generated from heterozygous *Igha*$^{+/-}$ parents exhibited an expansion of *Lactobacillus* and *S24-7* families belonging to *Bacteroidales*, a microbial order physiologically coated by IgA (*30*). Compared to control *Igha*$^{+/+}$ littermates, cohoused *Igha*$^{-/-}$ mice also displayed a possible depletion of *Lachnospiraceae* (Fig. 2G), some of which were recently shown to critically support homeostatic gut IgA responses in mice and undergo depletion in patients with IGAD (*10*, *32*, *33*). More evidence is needed to firmly demonstrate the involvement of microbiota-dependent mechanisms in the enhancement of postimmune systemic IgG production by gut IgA. However, current data may offer a blueprint for more detailed microbiota studies aimed at validating the proposed model. In this model, IgA would exert IgG-enhancing activity by limiting commensal antigen penetration across the gut barrier while supporting IgA-inducing communities.

IgA could affect IgG responses via gut commensals

Next, we asked whether the selective lack of mucosal secretory IgA (SIgA) could phenocopy global IGAD. Gut SIgA is absent in *Pigr*$^{-/-}$ mice, which lack the polymeric Ig receptor (pIgR) needed to transport dimeric IgA across intestinal epithelial cells (*3*, *34*). Given that IgA may undergo paracellular leakage in *Pigr*$^{-/-}$ mice (*35*), we first quantified IgA in the stool from these mice. Compared to control *Pigr*$^{+/+}$ littermates, *Pigr*$^{-/-}$ mice generated from heterozygous *Pigr*$^{+/-}$ parents displayed a severe loss of fecal IgA (fig. S3J). Consistently and similar to *Igha*$^{-/-}$ mice, *Pigr*$^{-/-}$ mice induced less plasma IgG1 to PPS 21 and 28 days following intraperitoneal immunization with Prevnar13 compared to WT controls (Fig. 2H).

Next, we tested whether the lateral transmission of IgA-coated gut commensals could restore antipneumococcal IgG responses in *Igha*$^{-/-}$ mice. Compared to control *Igha*$^{+/+}$ littermates, cohoused *Igha*$^{-/-}$ mice generated from heterozygous *Igha*$^{+/-}$ parents still mounted a weaker plasma IgG1 response to PPS 21 and 28 days following intraperitoneal immunization with Prevnar13 compared to control *Igha*$^{+/+}$ littermates (Fig. 2I). Moreover, cohoused *Igha*$^{-/-}$ mice mounted a weaker IgG3 response to PPS from Pneumovax23 7, 14, 21, and 28 days following intraperitoneal immunization (fig. S3K).

Considering that mucosa lumen–restricted IGAD was sufficient to decrease systemic IgG responses to PPS and knowing that IgA

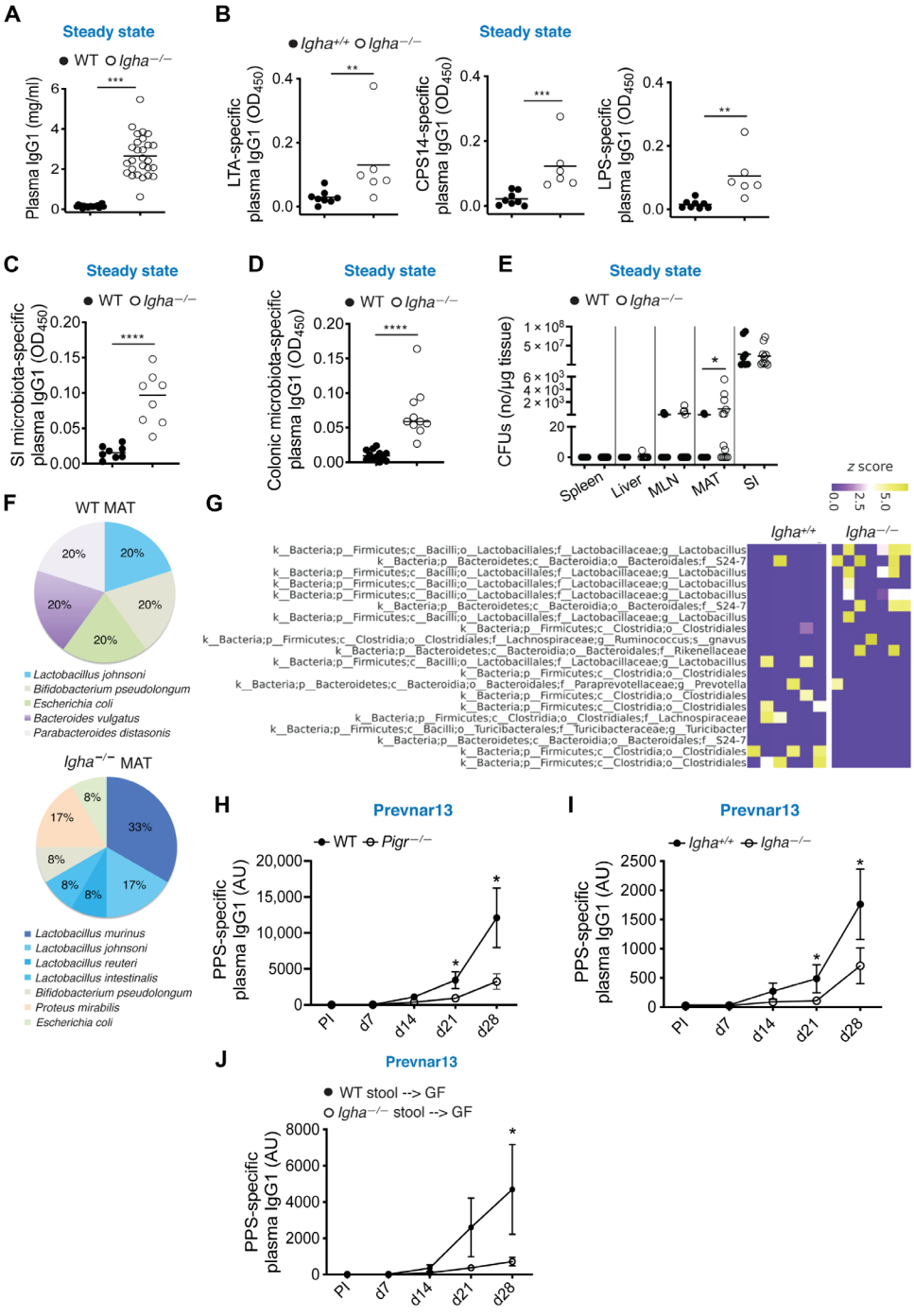

Fig. 2. IgA restrains preimmune IgG responses, including responses targeting gut commensal antigens. (**A**) ELISA of total steady-state plasma IgG1 from 20 WT or 27 *Igha*$^{-/-}$ mice. (**B**) ELISA of steady-state plasma IgG1 to LTA from *S. aureus*, CPS14 from *S. pneumoniae*, or LPS from *S. typhimurium* in eight *Igha*$^{+/+}$ or six *Igha*$^{-/-}$ littermate mice. (**C** and **D**) ELISA of plasma IgG1 to paired small intestine (SI) (C) or colon (D) fecal bacteria obtained from 8 to 12 WT or 8 to 10 *Igha*$^{-/-}$ mice. (**E**) Quantification of colony-forming units (CFUs) of anaerobic bacteria in homogenates of spleen, liver, mesenteric lymph nodes (MLNs), mesenteric adipose tissue (MAT), and SI from 8 to 13 WT or 9 to 13 *Igha*$^{-/-}$ mice. (**F**) Taxonomic classification of anaerobic bacterial colonies isolated from MAT from two WT or seven *Igha*$^{-/-}$ mice by mass spectrometry. (**G**) Top 10 differentially abundant amplicon sequence variants between six WT and seven *Igha*$^{-/-}$ cohoused littermate mice using analysis of composition of microbiomes (ANCOM) ($P < 0.05$) on 16*S* rRNA gene sequences of colonic feces. (**H**) ELISA of IgG1 to PPS from 9 WT mice or 10 *Pigr*$^{-/-}$ mice PI and following Prevnar13 intraperitoneally. (**I**) ELISA of IgG1 to PPS from 11 *Igha*$^{+/+}$ or 16 *Igha*$^{-/-}$ cohoused littermate mice from *Igha*$^{+/-}$ parents PI and following Prevnar13 intraperitoneally. (**J**) ELISA of IgG1 to PPS PI or following intraperitoneal immunization with Prevnar13 of ex-GF mice 2 weeks after reconstitution of six to seven GF recipient mice with specific pathogen–free WT or *Igha*$^{-/-}$ cecal content. Results summarize five [(A), (E), and (F)], one [(B), (G), and (J)], or two [(C), (D), (H), and (I)] independent experiments. Data are presented with mean [(A) to (E)] or as mean ± SEM [(H) to (J)]; two-tailed unpaired Student's *t* test used for normally distributed data otherwise Mann-Whitney test. *$P < 0.05$, **$P < 0.01$, ***$P < 0.001$, and ****$P < 0.0001$.

shapes the composition and function of the intestinal microbiota, we determined whether gut bacteria from *Igha*$^{-/-}$ mice had a negative impact on their antipneumococcal IgG response. Compared to ex-GF mice obtained by reconstituting GF recipients with fecal bacteria from WT mice, ex-GF mice obtained by reconstituting GF recipients with fecal bacteria from *Igha*$^{-/-}$ mice induced less IgG1 to PPS 28 days following intraperitoneal immunization with Prevnar13 (Fig. 2J). More studies are needed to conclusively demonstrate the involvement of the gut microbiota in the impaired postimmune IgG response observed in *Igha*$^{-/-}$ mice. However, the data shown here do suggest that IgA enhances systemic IgG responses to pneumococcal vaccines through mechanisms involving commensal microbes. Hypothetically, IgA may be crucial for the retention and early shaping of the immunometabolic properties of one or more communities of commensal bacteria with pronounced IgG-inducing function.

IgA controls FO B cell differentiation to PCs

Considering the importance of T follicular helper (T_{FH}) cells in B cell activation and IgG1 production (*36*), we explored whether GCs from gut-associated Peyer's patches (PPs), MLNs, and spleen of *Igha*$^{-/-}$ mice showed any B cell and/or T cell anomalies. Compared to WT controls, *Igha*$^{-/-}$ mice showed enlarged PPs and MLNs but normally sized spleen upon macroscopic analysis (Fig. 3A and fig. S4A). Accordingly, PPs and MLNs from *Igha*$^{-/-}$ mice had an increased cellularity, while the spleen did not (Fig. 3B). However, flow cytometry detected increased GC B cells and T_{FH} cells not only in PPs and MLNs but also in the spleen from *Igha*$^{-/-}$ mice (Fig. 3, C to F).

Given that IGAD caused an expansion of GC B cells in splenic follicles from *Igha*$^{-/-}$ mice, we characterized the global transcriptome of splenic FO cells from these mice. This study also included splenic MZ B cells, as IGAD impaired IgG responses to both TD and TI pneumococcal vaccines. RNA sequencing (RNA-seq) data visualized through volcano plots showed that FO B cells from *Igha*$^{-/-}$ mice had more differentially expressed genes (DEGs) than MZ B cells when compared to WT controls (Fig. 3G). In addition, gene set variation analysis (GSVA) showed that, compared to WT controls, FO B cells from *Igha*$^{-/-}$ mice expressed more gene sets linked to B cell proliferation, GC differentiation, and PC differentiation (Fig. 3H).

As shown by heatmaps of RNA-seq data (Fig. 3I), these increased gene sets included previously described transcripts (*37*) implicated in GC differentiation (e.g., *Tmem121*, *2510009E07Rik*, *Troap*, *Ncapg*, *Fscn1*, *Aicda*, and *Ighg1*) and PC differentiation (e.g., *Ncapg*, *Ccna2*, and *Shcbp1*). Having shown that *Igha*$^{-/-}$ mice have enhanced IgG1 responses to commensal antigens, we compared IgG1 class SBCs as well as IgG1-expressing PBs and PCs from *Igha*$^{-/-}$ mice and WT controls. By using a flow cytometric assay capable of distinguishing surface from intracellular IgG1, we determined that *Igha*$^{-/-}$ mice had more IgG1$^+$ SBCs, IgG1$^+$ PBs, and IgG1$^+$ PCs in the spleen as well as MLNs and PPs compared to WT controls (Fig. 3J and fig. S4, B and C).

Knowing that IgA starts influencing the intestinal microbiota soon after birth and that gut bacteria stimulate early postnatal immune development (*38*, *39*), we determined whether IGAD caused early immune anomalies. We found that both size and cellularity of MLNs were already increased in 5-week-old *Igha*$^{-/-}$ mice compared to WT controls (fig. S4D). Similar to adult mice, MLNs and spleen from 5-week-old *Igha*$^{-/-}$ mice included more total GC B cells, IgG1$^+$ GC B cells, T_{FH} cells, IgG1$^+$ SBCs, IgG1$^+$ PBs, and IgG1$^+$ PCs than WT controls (fig. S4, E and F). Accordingly, 5-week-old *Igha*$^{-/-}$ mice had more total plasma IgG1 than WT controls, and this increase was augmented in 14-week-old *Igha*$^{-/-}$ mice (fig. S4G). Like adult mice, 5-week-old *Igha*$^{-/-}$ mice further showed more plasma IgG1 to colonic gut microbiota than WT controls but less plasma IgG3 to TNP-Ficoll 5 days following intraperitoneal immunization (fig. S4, H and I). Thus, gut IgA may enhance systemic IgG responses to vaccines by constraining the differentiation of FO B cells into IgG-secreting PCs via the GC reaction and may start doing so at a very early age.

IgA constrains T cell expression of the immune inhibitor PD-1

Next, we hypothesized that, in the absence of IgA, the early and persistent exposure to systemically translocated gut antigens could impair peripheral IgG responses to vaccines by chronically activating B cells, which could lead to a state of functional B cell hyporesponsiveness similar to B cell anergy (*40*, *41*). Before addressing this point, we first investigated whether the FO B cell hyperactivation detected in *Igha*$^{-/-}$ mice was associated with any gut enrichment in proinflammatory segmented filamentous bacteria (SFB). It was recently reported that SFB are expanded in the SI of *Igha*$^{-/-}$ mice and contribute to its inflammation (*42*). Consistent with our earlier data showing no inflammation in the gut from *Igha*$^{-/-}$ mice, the SI, caecum, and colon from these mice showed similar SFB abundance to cohoused *Igha*$^{+/+}$ littermate controls (fig. S4J). This result, together with our earlier finding showing a persistently attenuated antipneumococcal IgG1 response in ex-GF mice reconstituted with cecal bacteria from *Igha*$^{-/-}$ donors, suggests that SFB are unlikely to be involved in the FO B cell hyperactivation detected in *Igha*$^{-/-}$ mice.

Then, we determined whether B cells from *Igha*$^{-/-}$ mice expressed a gene signature consistent with functional hyporesponsiveness. As shown by GSVA, splenic FO but not MZ B cells from *Igha*$^{-/-}$ mice were enriched in B cell anergy genes compared to WT controls (Fig. 4A). A heatmap visualization of DEGs selected on the basis of published findings (*40*) highlighted *Cenpv*, *Lef1*, *Nefh*, *Fabp5*, and *Tgif1* among several other gene products (Fig. 4B). Considering that the activation-induced receptor PD-1 transmits powerful inhibitory signals to activated B cells via PD-1 ligands (*43*), we also evaluated whether IGAD increased PD-1 and PD ligand 1 (PD-L1) expression on systemic T and B cells, respectively. Compared to WT controls, *Igha*$^{-/-}$ mice showed more PD-1$^+$CD4$^+$ and PD-1$^+$CD8$^+$ T cells, including antigen-experienced PD-1$^+$CD44$^+$CD4$^+$ and PD-1$^+$CD44$^+$CD8$^+$ T cells, in spleen and MLNs but not PPs (Fig. 4C and fig. S5A). Similar to adult *Igha*$^{-/-}$ mice, 5-week-old *Igha*$^{-/-}$ mice had more PD-1$^+$CD4$^+$ T cells, including antigen-experienced PD-1$^+$CD44$^+$CD4$^+$ T cells, in both spleen and MLNs (fig. S5B). Last, splenic MZ and B-1 but not FO B cells from *Igha*$^{-/-}$ mice exhibited increased PD-L1 expression compared to WT controls (Fig. 4D).

The involvement of PD-1 in the inhibition of vaccine-induced IgG1 was further evaluated using anti–PD-1. Anti–PD-1–treated *Igha*$^{-/-}$ mice intraperitoneally immunized with Prevnar13 showed significantly more plasma IgG1 to PPS at day 14 compared with isotype control–treated *Igha*$^{-/-}$ mice (Fig. 4E and fig. S5C). Anti–PD-1–treated *Igha*$^{-/-}$ mice also showed more plasma IgG1 to PPS at days 0 and 7 compared to anti–PD-1–treated WT controls (Fig. 4E and fig. S5C). This early response to anti–PD-1 treatment by *Igha*$^{-/-}$ mice likely contributed to the induction by immunized anti–PD-1–treated *Igha*$^{-/-}$ mice of as much plasma IgG1 to PPS at days 56 and 86 as isotype control–treated WT mice. In contrast, in line with our earlier findings, isotype control–treated *Igha*$^{-/-}$ mice intraperitoneally

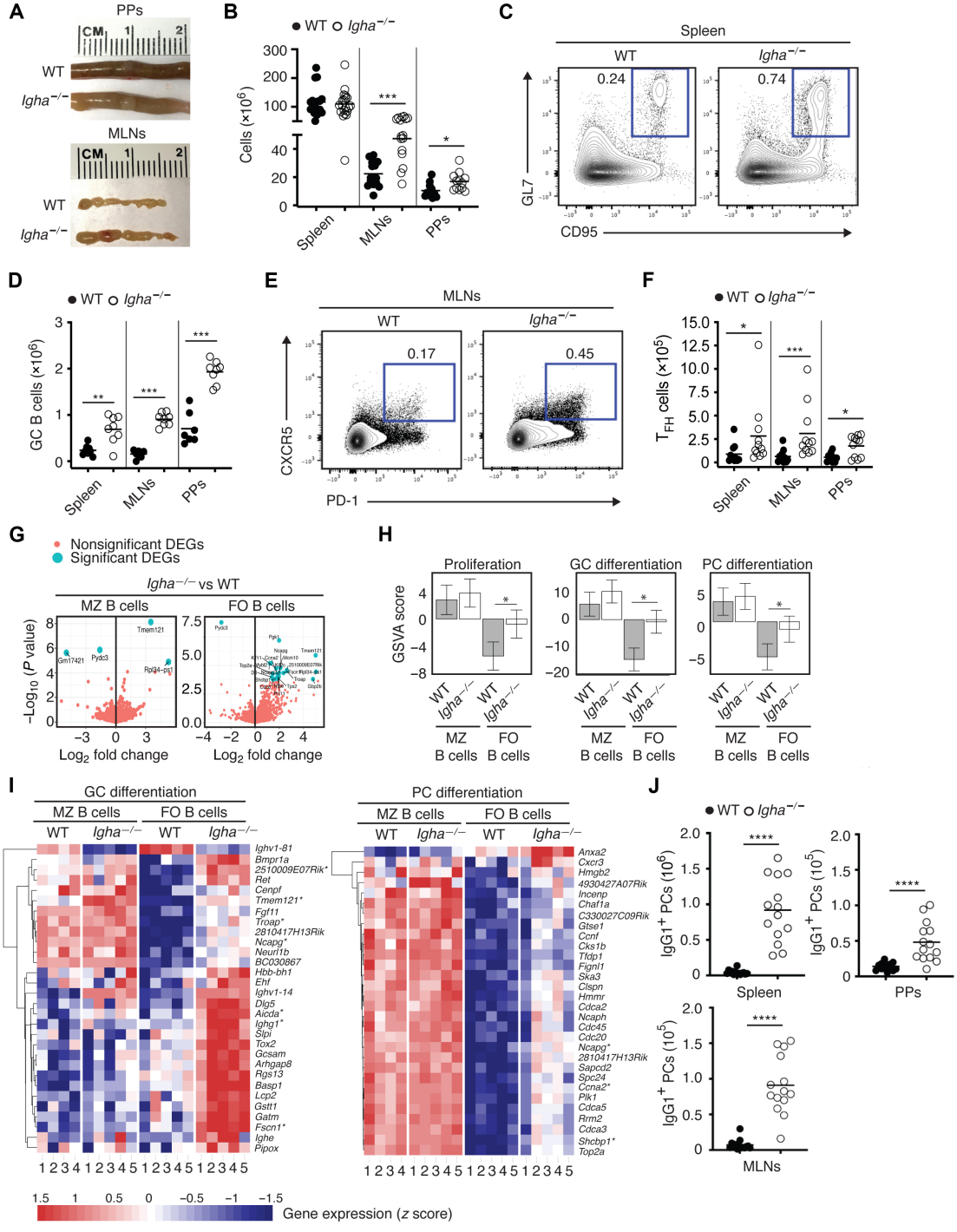

Fig. 3. IgA restrains IgG1$^+$ GC B cell expansion and IgG1$^+$ PC differentiation. (**A**) Images of PPs and MLNs from representative WT or *Igha*$^{-/-}$ mice. (**B**) Total cells in spleen, MLNs, and PPs from 11 to 19 WT or 12 to 20 *Igha*$^{-/-}$ mice. (**C** and **D**) Flow cytometry of splenic CD95$^+$GL7$^+$ GC B cells (live CD45$^+$B220$^+$ cells) from representative WT or *Igha*$^{-/-}$ mice (C) and absolute numbers in spleen, MLNs, and PPs from seven to eight WT or 8 *Igha*$^{-/-}$ mice. (**E** and **F**) PD-1$^+$CXCR5$^+$ T_{FH} cells (CD45$^+$CD19$^-$TCRβ$^+$CD4$^+$ cells) from MLNs of representative WT or *Igha*$^{-/-}$ mice (E) and absolute numbers in spleen, MLNs, and PPs from 10 to 11 WT or 11 *Igha*$^{-/-}$ mice (F). (**G**) Volcano plot of differentially expressed genes (DEGs) identified by RNA-seq in splenic MZ and FO B cell from four to five WT or five *Igha*$^{-/-}$ mice. (**H**) Gene set variation analysis (GSVA) of proliferation (G_2-M checkpoint) and GC and PC differentiation gene signatures identified by RNA-seq as in (G). (**I**) Heatmap of *z* score for top 30 DEGs related to GC (left) and PC differentiation (right) gene sets identified by RNA-seq as in (G). Asterisks indicate DEGs discussed in the text. The scale bar shows color coding for *z* score. (**J**) Absolute numbers of IgG1$^+$ PCs (IgD^{lo}CD45$^+$; fig. S4B) in spleen, MLNs, and PPs from 14 WT or *Igha*$^{-/-}$ mice. Data show representative images or flow plots [(A), (C), and (E)], summarize two (J), three (D), six (B), or one [(G) to (I)] independent experiments, or summarize three experiments representative of five (F). Data presented with mean [(B), (D), and (F)], median (J), or mean GSVA score and 95% confidence interval (H); two-tailed unpaired Student's *t* test used for normally distributed data otherwise Mann-Whitney test or limma modeling (H). *$P < 0.05$, **$P < 0.01$, ***$P < 0.001$, and ****$P < 0.0001$.

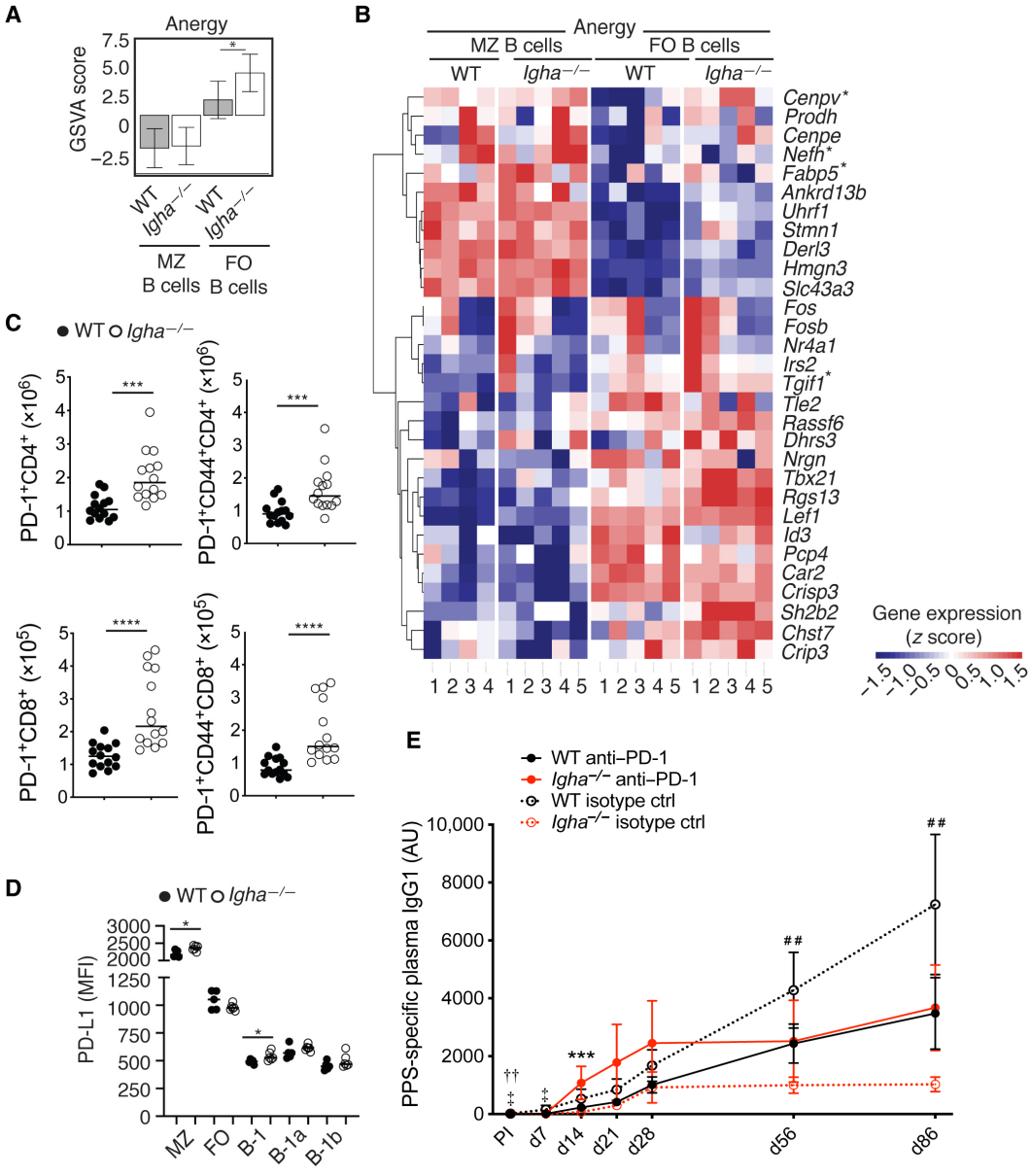

Fig. 4. IgA constrains activation-induced T cell expression of the immune inhibitor PD-1, and anti–PD-1 improves postimmune IgG production in IGAD. (**A**) GSVA of anergy gene signature identified by RNA-seq from splenic MZ and FO B cells from four to five WT or five *Igha*$^{-/-}$ mice at steady state. (**B**) Heatmap shows gene expression for top 30 DEGs from anergy gene set in (A). Asterisks indicate DEGs discussed in the text. The scale bar shows color coding for *z* score. (**C**) Absolute numbers of splenic PD-1^{+}CD4^{+} (top) or PD-1^{+}CD8^{+} (bottom) total (left) or antigen-experienced CD44^{+} (right) T cells from 14 WT or *Igha*$^{-/-}$ mice determined by flow cytometry. (**D**) PD-L1 [mean fluorescence intensity (MFI)] on splenic MZ B, FO B, total B-1, B-1a, and B-1b cells from five WT or six *Igha*$^{-/-}$ mice. (**E**) ELISA of plasma IgG1 to PPS PI and following Prevnar13 intraperitoneally of seven to eight WT or *Igha*$^{-/-}$ mice treated with anti–PD-1 or isotype control (ctrl) 1 day before and after immunization, followed by every third day through day 19. Results summarize one [(A), (B), and (D)] or two (C) independent experiments or show one experiment representative of two (E). Data are presented with mean GSVA score and 95% confidence interval (A), median (C), mean (D), or mean and SEM (E). Significance was determined using limma modeling (A) or Mann-Whitney test [(C) to (E)]. *$P < 0.05$, **$P < 0.01$, ***$P < 0.005$, and ****$P < 0.001$. In (E), # compares isotype ctrl WT and isotype ctrl *Igha*$^{-/-}$, * compares isotype ctrl *Igha*$^{-/-}$ and anti–PD-1 *Igha*$^{-/-}$, ‡ compares anti–PD-1 WT and anti–PD-1 *Igha*$^{-/-}$, and † compares WT isotype ctrl and anti–PD-1 WT.

immunized with Prevnar13 showed reduced plasma IgG1 to PPS at days 56 and 86 compared to isotype control–treated WT mice (Fig. 4E and fig. S5C).

IgA limits anergic B cells and gut permeability in humans

We also assessed whether IGAD increased gut commensal antigen penetration and peripheral B cell anergy in humans. Flow cytometry showed an increased although small fraction of phenotypically anergic IgM^{low}CD21^{low} naive B cells (*44*) in blood samples from a New York City (NYC) cohort of adult patients with IGAD compared to age-matched controls (Fig. 5A and table S2). In agreement with the lack of IgA, the frequency of switched memory B cells was decreased in patients with IGAD, whereas the frequency of circulating total, naive, and MZ-like B cells was normal (fig. S5D). These findings were

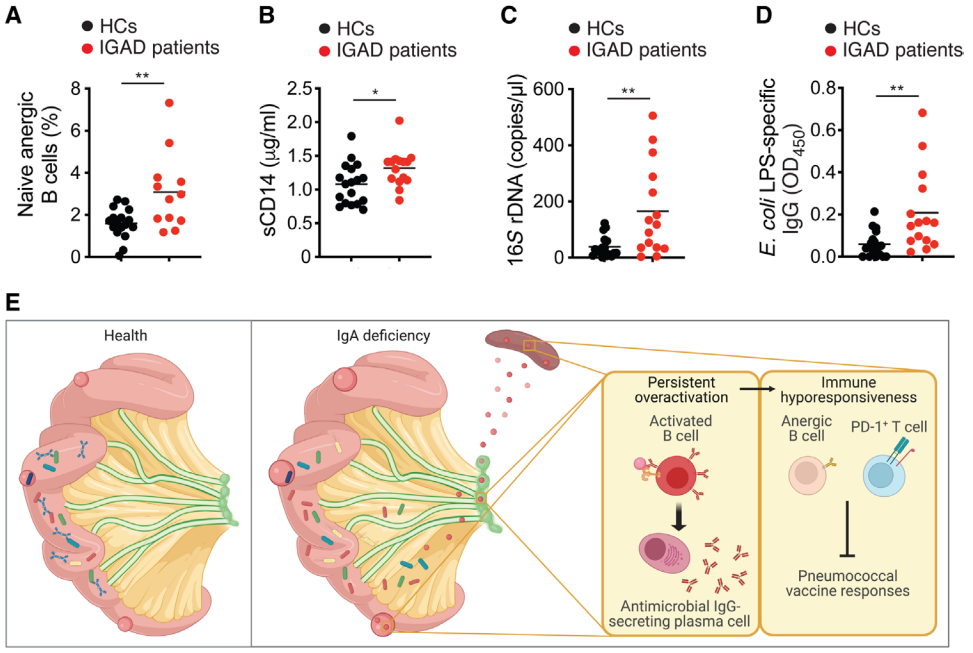

Fig. 5. IgA constrains the systemic translocation of gut commensal antigens. (**A**) Frequency (%) of circulating B cells with hyporesponsive-anergic IgM^{lo}CD21^{lo} phenotype within total IgD^{+}CD27^{-} naive B cell population from 17 HCs and 12 IgA-deficient (IGAD) patients. (**B**) ELISA of soluble (s)CD14 in plasma from 18 HCs and 15 patients with IGAD. (**C**) Quantitative PCR of bacterial 16*S* rDNA in plasma from 18 HCs and 15 patients with IGAD. (**D**) ELISA of IgG to LPS from *E. coli* in plasma from 18 HCs and 15 patients with IGAD. (**E**) Proposed model depicting the impact of gut IgA on systemic IgG responses to pneumococcal vaccines. Compared to the IgA-sufficient gut (left), the IgA-deficient gut (right) experiences increased penetration of viable gut commensals into the MAT due to the defective immune exclusion of intraluminal bacteria. The resulting peripheral penetration of soluble commensal antigens from MAT-based bacteria starts at an early age and leads to the chronic stimulation of the immune system, including B and T cells. B cells release progressively increasing amounts of IgG to gut commensal antigens (left inset), whereas T cells up-regulate PD-1 expression (right inset), respectively. Persistent B cell stimulation by gut antigens combined with enhanced B cell inhibitory signals from PD-1 could cause the functional exhaustion of systemic B cells, which would then become hyporesponsive to neoantigens from pneumococcal vaccines. Results summarize one experiment with multiple biological replicates. Data are presented with mean and significance determined using Mann-Whitney test. *$P < 0.05$ and **$P < 0.01$. (E) was created in BioRender.com.

replicated in a Barcelona (BCN) cohort of adult patients with IGAD, who also showed a lower frequency of IgA^{+} PCs (fig. S5E and table S3). An additional BCN cohort of IGAD pediatric patients similarly showed a decreased frequency of IgA^{+} PCs, which was accompanied by an increased frequency of IgG^{+} PCs but a normal frequency of switched memory B cells as well as total, naïve, and MZ-like B cells (fig. S5F and table S3). Thus, similar to *Igha*$^{-/-}$ mice, patients with IGAD showed IgA^{+} PC depletion combined with an increase of both "anergic" B cells and IgG^{+} PCs (*44*). The latter increase echoes the increased circulating IgG1 to gut commensal antigens found in *Igha*$^{-/-}$ mice. Accordingly, and in line with published findings (*8*, *10*, *45*), patients with IGAD from the NYC cohort showed signs of enhanced gut permeability, including more circulating soluble CD14 (sCD14), more bacterial 16*S* ribosomal DNA (rDNA), and more IgG to LPS from *Escherichia coli* compared to healthy controls (HCs; Fig. 5, B to D).

Thus, gut IgA enhances systemic IgG responses to pneumococcal vaccines. This positive effect would start soon after birth and could involve the limitation of commensal antigen penetration by IgA (Fig. 5E). Although more data are needed to validate the following model, we propose that, in the absence of IgA, enhanced infiltration of commensal antigens across the gut barrier elicits chronic IgG responses to these antigens. Over time, the resulting B and T cell hyperactivation would weaken IgG responses to neoantigens, including pneumococcal vaccines, via mechanisms possibly involving B cell hyporesponsiveness and T cell overexpression of PD-1.

DISCUSSION

We have shown that gut IgA positively affects systemic postimmune IgG responses to pneumococcal vaccines through a pathway already active soon after birth. IGAD is associated with increased gut antigen penetration along with systemic hyperactivation of both B and T cells, including exaggerated preimmune IgG responses to commensal antigens along with PD-1 overexpression. Together with B cell exhaustion, increased T cell expression of PD-1 may contribute to the attenuation of pneumococcal vaccine-induced IgG production. Thus, gut IgA amplifies systemic postimmune IgG responses through a mechanism that appears very early in life and could entail the intraluminal control of gut commensal antigens.

The gut microbiota enhances mucosal IgA and systemic IgG responses to a broad spectrum of bacteria (*7*, *8*, *46*, *47*), which leads to the generation of a preimmune layer of humoral protection against both noninvasive commensals and invasive pathogens (*16*, *47*, *48*). This dual function may stem from the cross-reactivity of some immunodominant antigens shared by commensals and pathogens (*16*, *47*, *48*). Consistently, patients with combined IgA and IgG deficiency are at increased risk of both systemic infections and gut inflammation (*8*, *9*).

Gut commensals also sustain specific systemic IgG responses to vaccines (*15*, *49*). Here, we hypothesized that this effect involves IgA, which extensively coats the gut microbiota (*30*, *32*). Consistent with this hypothesis, systemic IgG responses to pneumococcal vaccines are impaired in some patients with IGAD (*12*, *13*). By showing that IgA-deficient *Igha*$^{-/-}$ mice had severely impaired IgG responses to pneumococcal vaccines, our findings indicate that gut IgA is functionally linked to systemic IgG. Of note, *Igha*$^{-/-}$ mice showed impaired IgG responses to both Prevnar13 and Pneumovax23, two pneumococcal antigens that activate FO and MZ B cell subsets via distinct TD and TI pathways, respectively (*20*). These findings imply that gut IgA shapes antibody responses through multiple mechanisms, which may involve or not T cell help to B cells. While the impact of IgA was mostly dissected in relationship to systemic TD IgG responses, IgA may also regulate systemic TI IgG responses, as discussed later.

The link between gut IgA and systemic IgG may involve the gut microbiota, because pIgR-deficient *Pigr*$^{-/-}$ mice, which selectively lack intraluminal mucosal IgA (*34*), were found to mount an attenuated IgG response to the TD pneumococcal vaccine Prevnar13 compared to WT controls. The involvement of gut commensals was further suggested by the finding that GF recipient mice reconstituted with gut bacteria from *Igha*$^{-/-}$ donors mounted a weaker antipneumococcal IgG response compared to controls reconstituted with gut bacteria from WT donors. Although still incomplete and somewhat preliminary, these results do suggest the involvement of the gut microbiota in the impaired antipneumococcal IgG response observed in *Igha*$^{-/-}$ mice. More studies are clearly needed to conclusively demonstrate this involvement as well as relative impact of IGAD on protective IgG responses to specific CPSs. Of note, some of these microbial polysaccharides may be more sensitive to the lack of IgA than others.

Of note, the phenotype of *Pigr*$^{-/-}$ mice was milder compared to that of *Igha*$^{-/-}$ mice, which could stem from increased circulating dimeric IgA in *Pigr*$^{-/-}$ mice (*34*). Because of its inability to translocate across the gut epithelium, dimeric IgA progressively accumulates in the gut lamina propria of *Pigr*$^{-/-}$ mice (*34*). The ensuing increase of circulating dimeric IgA may enhance the clearance of systemically translocated gut commensal antigens in *Pigr*$^{-/-}$ mice compared to *Igha*$^{-/-}$ mice, which completely lack IgA (*23*). By attenuating the chronic hyperactivation and ensuing functional hyporesponsiveness of systemic B cells, this process could explain the less compromised antipneumococcal IgG response observed in *Pigr*$^{-/-}$ mice. An additional explanation may relate to nonspecific paracellular transfer of commensal-reactive IgA as a result of the leaky nature of the gut epithelium from *Pigr*$^{-/-}$ mice (*35*). In these mice, gut barrier dysfunction results from decreased zonulin-1, occluding, and claudin-1 expression, which is central to the functionality of intercellular tight junctions in the gut epithelium (*35*). However, in our facility, *Pigr*$^{-/-}$ mice showed massively reduced fecal IgA compared to *Pigr*$^{+/+}$ littermate controls. When persistent over time, chronically increased gut antigen translocation is associated with progressive immune activation and exhaustion, which has been shown to lead to hyporesponsiveness to neoantigens also from vaccines (*50*, *51*).

Similar to *Pigr*$^{-/-}$ mice, GF recipient mice receiving the gut microbiota from *Igha*$^{-/-}$ donors displayed a milder postimmune phenotype compared to *Igha*$^{-/-}$ mice, possibly because GF mice progressively restore their IgA response following recolonization. This gradual recovery of IgA production could attenuate the systemic translocation of commensal antigens across the gut epithelium over time upon recolonization. It must be also noted that, compared to the gut mucosa from *Igha*$^{-/-}$ mice, the gut mucosa from recolonized ex-GF mice is exposed to the microbiota from *Igha*$^{-/-}$ mice for a much shorter time, which may reduce the gut mucosa contact with dysbiotic bacterial communities.

Earlier works explored the impact of the gut microbiota on IgG responses to vaccines (*15*, *49*) but did not evaluate the contribution of IgA, which physiologically binds to intestinal microbes. This binding shapes both the composition and function of gut commensals, including their metabolic properties (*10*, *52*, *53*). Furthermore, IgA binding to gut bacteria maximizes microbiota diversity, which seems critical for optimal IgG responses to vaccines (*49*, *52*). Moreover, IgA confines gut microbes to the intestinal lumen, which limits their interaction with the immune system (*3*). Consistent with the involvement of IgA in shaping the composition of gut bacterial communities, IGAD enriched the microbiota in *Lactobacillaceae* among other smaller changes. This mild dysbiosis is consistent with published findings (*42*, *54*) and likely reflects compensatory effects brought about by the increased IgM and IgG production in the IgA-deficient gut (*26*, *55*). It must be also noted that small microbiota compositional differences may be associated with more profound microbiota functional changes, including motility changes that may not be detected by commonly used high-throughput screening approaches such as the 16*S* rDNA sequencing method used in our study (*53*).

Motility changes could be at the root of the abnormal MAT translocation of *L. murinus*, *L. reuteri*, and *L. intestinalis* detected in *Igha*$^{-/-}$ mice. The MAT-specific translocation of viable Lactobacilli may reflect both the role of MAT as gut antigen entry site and the role of IgA in the containment of commensals within the gut lumen (*56*). Accordingly, IgA has been shown to coat Lactobacilli (*30*). Of note, MAT-restricted bacterial translocation has also been observed in Crohn's disease and may relate to the swift engulfment of invading commensals by MAT phagocytes (*29*, *57*). Stromal cells and adipocytes would further help phagocytes to impede bacterial dissemination beyond the MAT (*57*, *58*), which likely explains our failure to detect more viable bacteria in MLNs as well as liver and spleen from *Igha*$^{-/-}$ mice.

Despite preventing MAT-based live bacteria from traveling to MLNs, liver, and spleen, phagocytosis would not impede the systemic penetration of soluble commensal antigens. In *Igha*$^{-/-}$ mice, this process could fuel persistent activation of peripheral B cells, which showed vastly augmented differentiation into GC B cells as well as PBs and PCs that released IgG1 to soluble microbial antigens, including CPS, LTA, and LPS. Of note, the increased systemic presence of gut commensal antigens was consistent with the detection of more bacterial 16*S* rDNA in both liver from *Igha*$^{-/-}$ mice and circulation from patients with IGAD.

In both *Igha*$^{-/-}$ mice and patients with IGAD, evidence suggesting enhanced gut antigen translocation was associated with evidence indicating overstimulation of both B and T cells. Accordingly, intestinal as well as systemic B cells from *Igha*$^{-/-}$ mice secreted more IgG1 and IgM to gut commensal antigens. These findings echo similar results from studies on patients with IGAD published while this work was under review (*26*, *55*). Because of the hyperactivation of splenic FO B cells, presumably caused by gut-derived commensal antigens, splenic GC B cells were increased in *Igha*$^{-/-}$ mice along

with GC-based T_{FH} cells. These mice also showed more activated antigen-experienced T cells expressing PD-1, an immune inhibitory receptor required for the fine tuning of IgA selection in gut GCs and for the compositional shaping of gut commensal communities to ensure host-microbiota symbiosis (*43*, *52*). A similar increase in $PD\text{-}1^{+}CD4^{+}$ T cells can be also detected in patients with IGAD (*10*). When treated with anti–PD-1, *Igha*$^{-/-}$ mice ameliorated their anti-pneumococcal IgG1 response, which points to the involvement of PD-1 in the hyporesponsiveness of FO B cells to vaccines.

Similar to *Igha*$^{-/-}$mice, patients with IGAD also showed an increased frequency of phenotypically exhausted $IgM^{low}CD21^{low}$ B cells. This increase was combined with augmented circulating sCD14, a soluble antigen released by myeloid cells following activation, including the activation induced by translocated commensal antigens (*10*, *45*). Thus, despite causing bacterial translocation largely restricted to the MAT, IGAD would chronically elicit systemic B cell hyperactivation and hyper-IgG1 production to commensal antigens through mechanisms that might entail the increased permeability of the intestinal mucosa and/or the increased motility or invasiveness of some commensals. Consistent with its capability to initiate antigen-specific IgG responses after intraperitoneal immunization (*59*, *60*), B cells from the MAT could be directly involved in the exaggerated commensal-specific IgG1 response observed in *Igha*$^{-/-}$mice.

At variance with a recently published study (*42*), the *Igha*$^{-/-}$mice from our colony showed no inflammation and no expansion of pro-inflammatory SFB in the SI and caecum compared to WT controls. Both inflammation and SFB expansion can stimulate gut IgG responses characterized by a strong IgG1 component (*19*, *27*, *28*). By showing that the abnormally high IgG1 production observed in *Igha*$^{-/-}$mice is coupled with neither gut inflammation nor SFB expansion, our findings support a model in which IgA enhances vaccine-specific IgG responses by constraining chronic B cell activation and the ensuing progressive B cell functional exhaustion. Although more evidence is needed, these two processes could result from the persistent penetration of commensal antigens across the IgA-deficient gut barrier and would account for the combination of preimmune hyper-IgG1 production and postimmune IgG1 deficiency in *Igha*$^{-/-}$ mice. Similar to these mice, some patients with IGAD show increased targeting of commensal bacteria by systemic IgG1 (*26*, *55*), which possibly stems from gut microbiota changes associated with a T_H2 cell–biased tissue microenvironment (*26*). In *Igha*$^{-/-}$ mice, increased preimmune IgG1 responses may have additional but not mutually exclusive explanations, including the lack of IgA-BCR signals outcompeting IgG-BCR signals in class–switched GC B cells from PPs (*61*). Regardless, more studies are warranted to investigate the impact of IgA on the other IgG subclasses constitutively increased in *Igha*$^{-/-}$ mice, including IgG2b and IgG3 previously shown to preferentially target the microbiota (*7*, *47*).

In addition to limiting T cell expression of PD-1, IgA constrained PD-L1 expression by B cells, as this ligand was increased on MZ B cells from *Igha*$^{-/-}$ mice. Unlike FO B cells, MZ B cells did not exhibit transcriptional signatures reflecting abnormal activation. Yet, their increased PD-L1 expression may initiate PD-1–mediated T cell inhibitory signals, which could promote the suppression of T_{FH} cells (*62*). The gut microbiota restrains signaling from PD-1 via inosine, a metabolite that modulates T cells through the adenosine A_{2A} receptor (*63*). Future studies should explore the possibility that IgA constrains T cell expression of PD-1 by supporting gut communities enriched in inosine-releasing commensals.

Although never systematically investigated, PD-1 also regulates TI IgG responses (*64*), which raises the possibility that PD-1–PD-L1 interaction contributes to the impairment of vaccine-induced TI in addition to TD IgG responses in *Igha*$^{-/-}$ mice. Such possibility echoes the recent detection of PD-1 expression on some bone marrow PCs (*65*). An alternative but not mutually exclusive possibility is that IGAD impairs TI IgG responses through PD-1–independent mechanisms involving gut metabolites. For instance, it could be hypothesized that *Igha*$^{-/-}$ mice experience an increased release of IgG-suppressing metabolites and/or decreased release of IgG-sustaining metabolites via a dysfunctional gut microbiota.

Cohousing experiments showed that the lateral transmission of a healthy gut microbiota into *Igha*$^{-/-}$ mice was not sufficient to rescue vaccine-specific IgG responses. Thus, it is plausible that IGAD irreversibly attenuates systemic IgG responses through a process that starts very early in life via vertical transmission of a dominant dysbiotic gut microbiota from the mother to the offspring. Accordingly, we found increased IgG1 responses to gut commensals as well as impaired IgG3 production to a PPS-mimicking TI immunogen in *Igha*$^{-/-}$ mice as early as 5 weeks after birth. These results echo published findings showing that early-life-origin B cells drive homeostatic gut IgA responses in the adult (*66*). They further reflect studies showing that gut IgA drives early microbiota changes and that gut microbes stimulate postnatal immune development (*38*, *39*). In this regard, IgA may function by optimizing gut retention of consortia with broad IgA-inducing properties, including *Lachnospiraceae* A2 (*33*).

A limitation of our study relates to the extensive differences existing between *Igha*$^{-/-}$ mice and patients with IGAD. While *Igha*$^{-/-}$ mice have an absolute IGAD, patients with IGAD retain minimal amounts of IgA. In addition, *Igha*$^{-/-}$ mice consistently express the same phenotype, whereas patients with IGAD range from asymptomatic individuals to patients with mild, moderate, or even severe gastrointestinal and/or respiratory disorders. Only symptomatic patients with IGAD were considered in this report, because they are the only patients with IGAD to come to hospital attention. Nonetheless, their study was helpful to validate in humans some of the findings obtained in *Igha*$^{-/-}$ mice. In this regard, this work is about the fundamental biology of gut IgA rather than the pathogenesis of IGAD. Another limitation of this study relates to the still preliminary nature of the evidence supporting the impact of the gut microbiota in the impaired IgG response to pneumococcal vaccines in *Igha*$^{-/-}$ mice. An additional limitation relates to the lack of conclusive evidence as to the impact of PD-1 in the impairment of postimmune IgG responses in IgA-deficient mice. This evidence should include the analysis of mice lacking PD-1 in addition to IgA.

In summary, we found that gut IgA amplifies systemic postimmune IgG responses, including pneumococcal vaccine-specific IgG production. This effect starts very early in life and involves but may not be limited to the preimmune control of B and T cell activation, including PD-1 expression, possibly through the limitation of gut antigen penetration. Aside from revealing a previously unidentified functional link between gut IgA and systemic IgG, our data indicate that the former should be always considered in studies delving into the impact of gut microbes on systemic immune responses, including vaccine-induced IgG production. Consistent with recent propositions (*67*), our data also support the potential benefit of oral IgA therapy in patients with IGAD and with impaired IgG responses to vaccines and further imply that such a therapy should initiate very early in life.

MATERIALS AND METHODS

Study design

This study was designed to dissect the impact of mucosal IgA on systemic IgG responses to human pneumococcal vaccines. Our hypothesis was that mucosal IgA optimized systemic IgG production. This hypothesis was based on the following considerations. First, some immunodeficient patients lacking IgA have a poor IgG response to pneumococcal vaccines. Second, IgA extensively binds to mucosal commensal bacteria, including intestinal microbes, which in turn are thought to positively influence vaccine-induced IgG production. We compared *Igha*$^{-/-}$ or *Pigr*$^{-/-}$ mice with WT controls to evaluate whether and how the lack of total or intraluminal IgA influenced systemic IgG responses to human pneumococcal vaccines. In addition, we studied peripheral IgG responses to vaccines in ex-GF mice recolonized with gut commensal bacteria from *Igha*$^{-/-}$ mice and WT controls. Moreover, we combined ex vivo high-throughput studies with in vivo treatment of mice by a blocking anti–PD-1 antibody to characterize the mechanism by which IgA enhances IgG production to a pneumococcal vaccine.

Most experiments were performed two to six times, showed good reproducibility, and were summarized by pooling the data from all the experiments. The following were the exceptions. The flow cytometric analysis following TNP-Ficoll immunization (fig. S2, H and I), the GF mice recolonization with gut commensal bacteria from *Igha*$^{-/-}$ and WT mice (Fig. 2J), PD-L1 expression flow experiment (Fig. 4D), and RNA-seq analysis of splenic MZ and FO B cells from *Igha*$^{-/-}$ and WT mice were performed once. Human sCD14 and *E. Coli* LPS-specific IgG was measured in one ELISA and 16S rDNA was measured in one quantitative PCR run on plasma collected at different time points (Fig. 5, B to D). The 16*S* rRNA gene sequencing analysis of the microbiota from colon feces of WT controls and *Igha*$^{-/-}$ mice (Fig. 2G) was performed once in a well-controlled experiment using cohoused littermates. As shown in supplementary figures, immunizations with *S. pneumoniae* and TNP-LPS, DC subset analysis, Pneumovax23 immunization of cohoused littermates, and TNP-Ficoll immunization in 5-week-old mice were performed once. Significant outliers in normally distributed data were determined using the Grubb's test with an α of 0.05 and excluded from analysis.

Human subjects

Blood samples from the NYC and BCN cohorts were collected from age- and sex-matched HCs and patients with IGAD at Icahn School of Medicine at Mount Sinai and Vall d'Hebrón Hospital, respectively (tables S2 and S3). The Institutional Review Board of these institutions approved the use of blood specimens under approval numbers 10338 (NYC cohort) as well as PR(AG)79/2014 (BCN cohort, adults) and PR(AMI)135/2014 (BCN cohort, children). Treating clinicians identified IgA-deficient subjects on the basis of meeting consensus diagnostic criteria for selective IGAD. The study was then introduced to the potential subject, and if interested, the subject was consented for the study. Consenting was done in a private room, and potential risks of participating in the study were reviewed as well as any questions that came up after reviewing the consent form. Individuals provided consent for one sample collection only.

Analysis of human blood and stool samples

For the phenotypic study of B cells by flow cytometry, blood was collected in sodium heparin blood collection tubes. Peripheral blood mononuclear cells were obtained from sodium heparinized blood samples by separation on Ficoll Histopaque-1077 gradient (Sigma-Aldrich).

Mice

C57BL/6J (the Jackson Laboratory), *Igha*$^{-/-}$ (*23*), and *Pigr*$^{-/-}$ mice (*34*) were bred in the animal facility of Icahn School of Medicine at Mount Sinai and Weill Cornell Medicine under specific pathogen–free conditions. *Igha*$^{-/-}$ mice were obtained from Sergio Lira (Icahn School of Medicine at Mount Sinai), whereas *Pigr*$^{-/-}$ mice were provided by B. Garvy (University of Kentucky). WT and *Igha*$^{-/-}$ strains were generated by mating heterozygous *Igha*$^{+/-}$ parents to control for microbiota and genetic background variability between strains. WT mice used came from these strains, unless indicated otherwise. Similarly, WT and *Pigr*$^{-/-}$ strains were generated by mating heterozygous *Pigr*$^{+/-}$ parents. Both sexes were used, and mice were 4 to 16 weeks old for steady-state experiments and 5 to 12 weeks old for immunization experiments. All animal experiments described in this study were approved by Institutional Animal Care and Use Committee of the Icahn School of Medicine at Mount Sinai or Weill Cornell Medicine and were performed in accordance with the approved guidelines for animal experimentation at the Icahn School of Medicine at Mount Sinai and Weill Cornell Medicine. GF C57BL/6J mice were bred in-house at the Mount Sinai Immunology Institute Gnotobiotic Facility in flexible vinyl isolators. To facilitate high-throughput studies in gnotobiotic mice, "out-of-the-isolator" gnotobiotic techniques were used (*68*). Shortly after weaning and under strict aseptic conditions, 28- to 42-day-old GF mice were transferred to autoclaved filter-top cages outside of the breeding isolator and colonized with murine microbiota.

Analysis of murine blood and stool samples

Murine blood and stool samples were collected and analyzed as detailed in Supplementary Materials and Methods.

Colonization of GF mice

GF mice were reconstituted with fecal bacteria from WT or *Igha*$^{-/-}$ mice as detailed in Supplementary Materials and Methods.

Isolation and identification of translocated gut bacteria

Translocated gut bacteria were quantified and identified as detailed in Supplementary Materials and Methods.

Culture of bacteria

S. pneumoniae was cultured as detailed in Supplementary Materials and Methods.

Immunizations

Each mouse was intravenously or intraperitoneally immunized as detailed in Supplementary Materials and Methods and table S4.

Bacteria isolation from mouse feces

Fecal pellets collected directly from mice or from the SI were homogenized in phosphate-buffered saline (PBS; 1 ml/0.1 g) by vortexing for 10 min at room temperature. Suspension was centrifuged twice at 2000 rpm for 5 min at 4°C, and supernatants were collected. After centrifugation at 8000*g* for 10 min at 4°C, the supernatant was collected to measure free fecal IgM and IgG1. Resulting bacterial pellets were used to determine microbiota-specific IgG1 (see Supplementary Materials and Methods).

Flow cytometry and cell sorting

A total of 1 to 5 × 10^6 cells per sample were resuspended in PBS with Fc Block and Live/Dead staining. Cells were then washed with

fluorescence-activated cell sorting buffer (PBS with 2% heat-inactivated fetal bovine serum and 2 mM EDTA) and subsequently stained with extracellular antibodies. Intracellular IgG3/IgG1 was stained in permeabilization buffer after fixation and permeabilization as detailed in Supplementary Materials and Methods and table S4.

Enzyme-linked immunosorbent assay

Total or antigen-specific antibody subclasses, including high-affinity and low-affinity antibodies specific to NP and microbiota-reactive antibodies, as well as sCD14 were quantified as detailed in Supplementary Materials and Methods and table S4.

RNA sequencing

RNA was extracted from sorted splenic murine MZ and FO B cells using the QIAshredder and the RNeasy Plus Micro Kit (QIAGEN). Library preparation and sequencing were performed by a specialized company (GENEWIZ). RNA-seq analysis was performed as detailed in Supplementary Materials and Methods. RNA-seq sequence data files (fastq) are stored in the public sequence read archive (SRA) under project number PRJNA725246.

16*S* rRNA gene sequencing and analysis

DNA extraction using a ZYMO fecal DNA mini prep kit, library preparation, and 16*S* rRNA gene amplicon sequencing of colonic fecal bacteria from cohoused littermate *Igha*$^{+/+}$ and *Igha*$^{-/-}$ mice were outsourced (GENEWIZ), and analysis was done as detailed in Supplementary Materials and Methods. 16*S* sequence data files (fastq) are stored in the public SRA under accession number PRJNA722766.

16*S* rRNA gene quantitative PCR

DNA from mouse spleen, liver, and MLN, and from human plasma was extracted using the DNeasy Blood and Tissue Kit (QIAGEN), and 16*S* rRNA gene was amplified by quantitative PCR as detailed in Supplementary Materials and Methods and table S4 (*69*).

Mouse B cell cultures

Mouse B cells were cultured as detailed in Supplementary Materials and Methods and table S4.

Histology and immunofluorescence

Colon and SI from WT or *Igha*$^{-/-}$ mice were processed as detailed in Supplementary Materials and Methods.

Statistical analysis

Statistical analysis was performed using Prism version 9.0 (GraphPad). Comparisons between two groups were determined using either Student's *t* test when data followed a normal distribution or Mann-Whitney *U* test when data were not normally distributed. Normal Gaussian distribution was determined by a D'Agostino and Pearson normality test. For multiple comparisons, a Kruskal-Wallis test with Dunn's correction was used. For normally distributed data, significant outliers were determined using the Grubb's test with an α of 0.05 and excluded from analysis. A P value < 0.05 was considered significant. P values are indicated on plots and in figure legends. ($*P < 0.05$, $**P < 0.01$, $***P < 0.001$, and $****P < 0.0001$). Statistical analysis of 16S *r*RNA gene sequencing and RNA-seq is detailed in Supplementary Materials and Methods.

Supplementary Materials

The PDF file includes:

Supplementary Materials and Methods
Figs. S1 to S5
Tables S1 to S3
Legends for tables S4 and S5
References

Other Supplementary Material for this manuscript includes the following:

Tables S4 and S5

REFERENCES AND NOTES

1. Y. Belkaid, T. W. Hand, Role of the microbiota in immunity and inflammation. *Cell* **157**, 121–141 (2014).
2. S. E. De Jong, A. Olin, B. Pulendran, The impact of the microbiome on immunity to vaccination in humans. *Cell Host Microbe* **28**, 169–179 (2020).
3. K. Chen, G. Magri, E. K. Grasset, A. Cerutti, Rethinking mucosal antibody responses: IgM, IgG and IgD join IgA. *Nat. Rev. Immunol.* **20**, 427–441 (2020).
4. J. J. Bunker, T. M. Flynn, J. C. Koval, D. G. Shaw, M. Meisel, B. D. McDonald, I. E. Ishizuka, A. L. Dent, P. C. Wilson, B. Jabri, D. A. Antonopoulos, A. Bendelac, Innate and adaptive humoral responses coat distinct commensal bacteria with immunoglobulin A. *Immunity* **43**, 541–553 (2015).
5. E. K. Grasset, A. Chorny, S. Casas-Recasens, C. Gutzeit, G. Bongers, I. Thomsen, L. Chen, Z. He, D. B. Matthews, M. A. Oropallo, P. Veeramreddy, M. Uzzan, A. Mortha, J. Carrillo, B. S. Reis, M. Ramanujam, J. Sintes, G. Magri, P. J. Maglione, C. Cunningham-Rundles, R. J. Bram, J. Faith, S. Mehandru, O. Pabst, A. Cerutti, Gut T cell-independent IgA responses to commensal bacteria require engagement of the TACI receptor on B cells. *Sci. Immunol.* **5**, eaat7117 (2020).
6. A. M. Weis, J. L. Round, Microbiota-antibody interactions that regulate gut homeostasis. *Cell Host Microbe* **29**, 334–346 (2021).
7. M. A. Koch, G. L. Reiner, K. A. Lugo, L. S. M. Kreuk, A. G. Stanbery, E. Ansaldo, T. D. Seher, W. B. Ludington, G. M. Barton, Maternal IgG and IgA antibodies dampen mucosal T helper cell responses in early life. *Cell* **165**, 827–841 (2016).
8. J. Fadlallah, D. Sterlin, C. Fieschi, C. Parizot, K. Dorgham, H. El Kafsi, G. Autaa, P. Ghillani-Dalbin, C. Juste, P. Lepage, M. Malphettes, L. Galicier, D. Boutboul, K. Clément, S. André, F. Marquet, C. Tresallet, A. Mathian, M. Miyara, E. Oksenhendler, Z. Amoura, H. Yssel, M. Larsen, G. Gorochov, Synergistic convergence of microbiota-specific systemic IgG and secretory IgA. *J. Allergy Clin. Immunol.* **143**, 1575–1585.e4 (2019).
9. M. Uzzan, H. M. Ko, S. Mehandru, C. Cunningham-Rundles, Gastrointestinal disorders associated with common variable immune deficiency (CVID) and chronic granulomatous disease (CGD). *Curr. Gastroenterol. Rep.* **18**, 17 (2016).
10. J. Fadlallah, H. El Kafsi, D. Sterlin, C. Juste, C. Parizot, K. Dorgham, G. Autaa, D. Gouas, M. Almeida, P. Lepage, N. Pons, E. Le Chatelier, F. Levenez, S. Kennedy, N. Galleron, J.-P. P. De Barros, M. Malphettes, L. Galicier, D. Boutboul, A. Mathian, M. Miyara, E. Oksenhendler, Z. Amoura, J. Doré, C. Fieschi, S. D. Ehrlich, M. Larsen, G. Gorochov, Microbial ecology perturbation in human IgA deficiency. *Sci. Transl. Med.* **10**, eaan1217 (2018).
11. N. J. Croucher, A. Løchen, S. D. Bentley, Pneumococcal vaccines: Host interactions, population dynamics, and design principles. *Annu Rev Microbiol* **72**, 521–549 (2018).
12. P. J. Lane, I. C. MacLennan, Impaired IgG2 anti-pneumococcal antibody responses in patients with recurrent infection and normal IgG2 levels but no IgA. *Clin. Exp. Immunol.* **65**, 427–433 (1986).
13. E. Edwards, S. Razvi, C. Cunningham-Rundles, IgA deficiency: Clinical correlates and responses to pneumococcal vaccine. *Clin. Immunol.* **111**, 93–97 (2004).
14. A. Aghamohammadi, J. Mohammadi, N. Parvaneh, N. Rezaei, M. Moin, T. Espanol, L. Hammarstrom, Progression of selective IgA deficiency to common variable immunodeficiency. *Int. Arch. Allergy Immunol.* **147**, 87–92 (2008).
15. J. Z. Oh, R. Ravindran, B. Chassaing, F. A. Carvalho, M. S. Maddur, M. Bower, P. Hakimpour, K. P. Gill, H. I. Nakaya, F. Yarovinsky, R. B. Sartor, A. T. Gewirtz, B. Pulendran, TLR5-mediated sensing of gut microbiota is necessary for antibody responses to seasonal influenza vaccination. *Immunity* **41**, 478–492 (2014).
16. T. C. Cullender, B. Chassaing, A. Janzon, K. Kumar, C. E. Muller, J. J. Werner, L. T. Angenent, M. E. Bell, A. G. Hay, D. A. Peterson, J. Walter, M. Vijay-Kumar, A. T. Gewirtz, R. E. Ley, Innate and adaptive immunity interact to quench microbiome flagellar motility in the gut. *Cell Host Microbe* **14**, 571–581 (2013).
17. M. Kim, Y. Qie, J. Park, C. H. Kim, Gut microbial metabolites fuel host antibody responses. *Cell Host Microbe* **20**, 202–214 (2016).
18. Y. Uchimura, T. Fuhrer, H. Li, M. A. Lawson, M. Zimmermann, B. Yilmaz, J. Zindel, F. Ronchi, M. Sorribas, S. Hapfelmeier, S. C. Ganal-Vonarburg, M. Gomez De Agüero, K. D. McCoy, U. Sauer, A. J. Macpherson, Antibodies set boundaries limiting microbial metabolite penetration and the resultant mammalian host response. *Immunity* **49**, 545–559.e5 (2018).

19. M. Uzzan, J. C. Martin, L. Mesin, A. E. Livanos, T. Castro-Dopico, R. Huang, F. Petralia, G. Magri, S. Kumar, Q. Zhao, A. K. Rosenstein, M. Tokuyama, K. Sharma, R. Ungaro, R. Kosoy, D. Jha, J. Fischer, H. Singh, M. E. Keir, N. Ramamoorthi, W. E. O'Gorman, B. L. Cohen, A. Rahman, F. Cossarini, A. Seki, L. Leyre, S. T. Vaquero, S. Gurunathan, E. K. Grasset, B. Losic, M. Dubinsky, A. J. Greenstein, Z. Gottlieb, P. Legnani, J. George, H. Irizar, A. Stojmirovic, C. Brodmerkel, A. Kasarkis, B. E. Sands, G. Furtado, S. A. Lira, Z. K. Tuong, H. M. Ko, A. Cerutti, C. O. Elson, M. R. Clatworthy, M. Merad, M. Suárez-Fariñas, C. Argmann, J. A. Hackney, G. D. Victora, G. J. Randolph, E. Kenigsberg, J. F. Colombel, S. Mehandru, Ulcerative colitis is characterized by a plasmablast-skewed humoral response associated with disease activity. *Nat Med* **28**, 766–779 (2022).
20. A. Cerutti, M. Cols, I. Puga, Marginal zone B cells: Virtues of innate-like antibody-producing lymphocytes. *Nat. Rev. Immunol.* **13**, 118–132 (2013).
21. R. D. Astronomo, D. R. Burton, Carbohydrate vaccines: Developing sweet solutions to sticky situations? *Nat. Rev. Drug Discov.* **9**, 308–324 (2010).
22. P. V. Licciardi, A. Balloch, F. M. Russell, R. L. Burton, J. Lin, M. H. Nahm, E. K. Mulholland, M. L. K. Tang, Pneumococcal polysaccharide vaccine at 12 months of age produces functional immune responses. *J. Allergy Clin. Immunol.* **129**, 794–800.e2 (2012).
23. G. R. Harriman, M. Bogue, P. Rogers, M. Finegold, S. Pacheco, A. Bradley, Y. Zhang, I. N. Mbawuike, Targeted deletion of the IgA constant region in mice leads to IgA deficiency with alterations in expression of other Ig isotypes. *J. Immunol.* **162**, 2521–2529 (1999).
24. E. J. Pone, J. Zhang, T. Mai, C. A. White, G. Li, J. K. Sakakura, P. J. Patel, A. Al-Qahtani, H. Zan, Z. Xu, P. Casali, BCR-signalling synergizes with TLR-signalling for induction of AID and immunoglobulin class-switching through the non-canonical NF-κB pathway. *Nat. Commun.* **3**, 767 (2012).
25. M. Kobayashi, T. Pilishvili, J. L. Farrar, A. J. Leidner, R. Gierke, N. Prasad, P. Moro, D. Campos-Outcalt, R. L. Morgan, S. S. Long, K. A. Poehling, A. L. Cohen, Pneumococcal vaccine for adults aged ≥19 years: Recommendations of the advisory committee on immunization practices, United States, 2023. *MMWR Recomm. Rep.* **72**, 1–39 (2023).
26. C. Eriksen, J. M. Moll, P. N. Myers, A. R. A. Pinto, N. B. Danneskiold-Samsøe, R. I. Dehli, L. B. Rosholm, M. D. Dalgaard, J. Penders, D. M. Jonkers, Q. Pan-Hammarström, L. Hammarström, K. Kristiansen, S. Brix, IgG and IgM cooperate in coating of intestinal bacteria in IgA deficiency. *Nat. Commun.* **14**, 8124 (2023).
27. S. Verma, M. J. Dufort, T. M. Olsen, S. Kimmel, J. C. Labuda, S. Scharffenberger, A. T. McGuire, O. J. Harrison, Antigen-level resolution of commensal-specific B cell responses can be enabled by phage display screening coupled with B cell tetramers. *Immunity* **57**, 1428–1441.e8 (2024).
28. T. Castro-Dopico, T. W. Dennison, J. R. Ferdinand, R. J. Mathews, A. Fleming, D. Clift, B. J. Stewart, C. Jing, K. Strongili, L. I. Labzin, E. J. M. Monk, K. Saeb-Parsy, C. E. Bryant, S. Clare, M. Parkes, M. R. Clatworthy, Anti-commensal IgG drives intestinal inflammation and type 17 immunity in ulcerative colitis. *Immunity* **50**, 1099–1114.e10 (2019).
29. C. W. Y. Ha, A. Martin, G. D. Sepich-Poore, B. Shi, Y. Wang, K. Gouin, G. Humphrey, K. Sanders, Y. Ratnayake, K. S. L. Chan, G. Hendrick, J. R. Caldera, C. Arias, J. E. Moskowitz, S. J. Ho Sui, S. Yang, D. Underhill, M. J. Brady, S. Knott, K. Kaihara, M. J. Steinbaugh, H. Li, D. P. B. McGovern, R. Knight, P. Fleshner, S. Devkota, Translocation of viable gut microbiota to mesenteric adipose drives formation of creeping fat in humans. *Cell* **183**, 666–683.e17 (2020).
30. N. W. Palm, M. R. de Zoete, T. W. Cullen, N. A. Barry, J. Stefanowski, L. Hao, P. H. Degnan, J. Hu, I. Peter, W. Zhang, E. Ruggiero, J. H. Cho, A. L. Goodman, R. A. Flavell, Immunoglobulin A coating identifies colitogenic bacteria in inflammatory bowel disease. *Cell* **158**, 1000–1010 (2014).
31. Q. Zhao, S. N. Harbour, R. Kolde, I. J. Latorre, H. M. Tun, T. R. Schoeb, H. Turner, J. J. Moon, E. Khafipour, R. J. Xavier, C. T. Weaver, C. O. Elson, Selective induction of homeostatic Th17 cells in the murine intestine by cholera toxin interacting with the microbiota. *J. Immunol.* **199**, 312–322 (2017).
32. G. Magri, L. Comerma, M. Pybus, J. Sintes, D. Lligé, D. Segura-Garzón, S. Bascones, A. Yeste, E. K. Grasset, C. Gutzeit, M. Uzzan, M. Ramanujam, M. C. van Zelm, R. Albero-González, I. Vazquez, M. Iglesias, S. Serrano, L. Márquez, E. Mercade, S. Mehandru, A. Cerutti, Human secretory IgM emerges from plasma cells clonally related to gut memory B cells and targets highly diverse commensals. *Immunity* **47**, 118–134.e8 (2017).
33. S. Zhang, Y. Han, W. Schofield, M. Nicosia, P. E. Karell, K. P. Newhall, J. Y. Zhou, R. J. Musich, S. Pan, A. Valujskikh, N. Sangwan, M. Dwidar, Q. Lu, T. S. Stappenbeck, Select symbionts drive high IgA levels in the mouse intestine. *Cell Host Microbe* **31**, 1620–1638.e7 (2023).
34. F.-E. Johansen, M. Pekna, I. N. Norderhaug, B. Haneberg, M. A. Hietala, P. Krajci, C. Betsholtz, P. Brandtzaeg, Absence of epithelial immunoglobulin a transport, with increased mucosal leakiness, in polymeric immunoglobulin receptor/secretory component–deficient mice. *J. Exp. Med.* **190**, 915–922 (1999).
35. H. Lin, J. Lin, T. Pan, T. Li, H. Jiang, Y. Fang, Y. Wang, F. Wu, J. Huang, H. Zhang, D. Chen, Y. Chen, Polymeric immunoglobulin receptor deficiency exacerbates autoimmune hepatitis by inducing intestinal dysbiosis and barrier dysfunction. *Cell Death Dis.* **14**, 68 (2023).
36. S. Crotty, T follicular helper cell biology: A decade of discovery and diseases. *Immunity* **50**, 1132–1148 (2019).
37. W. Shi, Y. Liao, S. N. Willis, N. Taubenheim, M. Inouye, D. M. Tarlinton, G. K. Smyth, P. D. Hodgkin, S. L. Nutt, L. M. Corcoran, Transcriptional profiling of mouse B cell terminal differentiation defines a signature for antibody-secreting plasma cells. *Nat. Immunol.* **16**, 663–673 (2015).
38. J. D. Planer, Y. Peng, A. L. Kau, L. V. Blanton, I. M. Ndao, P. I. Tarr, B. B. Warner, J. I. Gordon, Development of the gut microbiota and mucosal IgA responses in twins and gnotobiotic mice. *Nature* **534**, 263–266 (2016).
39. M. Gomez de Agüero, S. C. Ganal-Vonarburg, T. Fuhrer, S. Rupp, Y. Uchimura, H. Li, A. Steinert, M. Heikenwalder, S. Hapfelmeier, U. Sauer, K. D. McCoy, A. J. Macpherson, The maternal microbiota drives early postnatal innate immune development. *Science* **351**, 1296–1302 (2016).
40. Z. Sabouri, S. Perotti, E. Spierings, P. Humburg, M. Yabas, H. Bergmann, K. Horikawa, C. Roots, S. Lambe, C. Young, T. D. Andrews, M. Field, A. Enders, J. H. Reed, C. C. Goodnow, IgD attenuates the IgM-induced anergy response in transitional and mature B cells. *Nat. Commun.* **7**, 13381 (2016).
41. J. C. Cambier, S. B. Gauld, K. T. Merrell, B. J. Vilen, B-cell anergy: From transgenic models to naturally occurring anergic B cells? *Nat. Rev. Immunol.* **7**, 633–643 (2007).
42. T. Nagaishi, T. Watabe, K. Kotake, T. Kumazawa, T. Aida, K. Tanaka, R. Ono, F. Ishino, T. Usami, T. Miura, S. Hirakata, H. Kawasaki, N. Tsugawa, D. Yamada, K. Hirayama, S. Yoshikawa, H. Karasuyama, R. Okamoto, M. Watanabe, R. S. Blumberg, T. Adachi, Immunoglobulin A-specific deficiency induces spontaneous inflammation specifically in the ileum. *Gut* **71**, 487–496 (2022).
43. T. Okazaki, T. Honjo, PD-1 and PD-1 ligands: From discovery to clinical application. *Int. Immunol.* **19**, 813–824 (2007).
44. J. A. Duty, P. Szodoray, N.-Y. Zheng, K. A. Koelsch, Q. Zhang, M. Swiatkowski, M. Mathias, L. Garman, C. Helms, B. Nakken, K. Smith, A. D. Farris, P. C. Wilson, Functional anergy in a subpopulation of naive B cells from healthy humans that express autoreactive immunoglobulin receptors. *J. Exp. Med.* **206**, 139–151 (2009).
45. J. M. Brenchley, D. C. Douek, Microbial translocation across the GI tract. *Annu. Rev. Immunol.* **30**, 149–173 (2012).
46. E. Ansaldo, L. C. Slayden, K. L. Ching, M. A. Koch, N. K. Wolf, D. R. Plichta, E. M. Brown, D. B. Graham, R. J. Xavier, J. J. Moon, G. M. Barton, Akkermansia muciniphila induces intestinal adaptive immune responses during homeostasis. *Science* **364**, 1179–1184 (2019).
47. M. Y. Zeng, D. Cisalpino, S. Varadarajan, J. Hellman, H. S. Warren, M. Cascalho, N. Inohara, G. Núñez, Gut microbiota-induced immunoglobulin G controls systemic infection by symbiotic bacteria and pathogens. *Immunity* **44**, 647–658 (2016).
48. T. Rollenske, V. Szijarto, J. Lukasiewicz, L. M. Guachalla, K. Stojkovic, K. Hartl, L. Stulik, S. Kocher, F. Lasitschka, M. Al-Saeedi, J. Schröder-Braunstein, M. von Frankenberg, G. Gaebelein, P. Hoffmann, S. Klein, K. Heeg, E. Nagy, G. Nagy, H. Wardemann, Cross-specificity of protective human antibodies against Klebsiella pneumoniae LPS O-antigen. *Nat. Immunol.* **19**, 617–624 (2018).
49. T. Hagan, M. Cortese, N. Rouphael, C. Boudreau, C. Linde, M. S. Maddur, J. Das, H. Wang, J. Guthmiller, N.-Y. Zheng, M. Huang, A. A. Uphadhyay, L. Gardinassi, C. Petitdemange, M. P. McCullough, S. J. Johnson, K. Gill, B. Cervasi, J. Zou, A. Bretin, M. Hahn, A. T. Gewirtz, S. E. Bosinger, P. C. Wilson, S. Li, G. Alter, S. Khurana, H. Golding, B. Pulendran, Antibiotics-driven gut microbiome perturbation alters immunity to vaccines in humans. *Cell* **178**, 1313–1328.e13 (2019).
50. M. H. El-Sayed, J. J. Feld, Vaccination at the forefront of the fight against hepatitis B and C. *Nat. Rev. Gastroenterol. Hepatol.* **19**, 87–88 (2022).
51. M. A. Ingersoll, Does immune cell exhaustion lie at the heart of BCG-unresponsive disease? *Nat. Rev. Urol.* **20**, 201–202 (2023).
52. S. Kawamoto, T. H. Tran, M. Maruya, K. Suzuki, Y. Doi, Y. Tsutsui, L. M. Kato, S. Fagarasan, The inhibitory receptor PD-1 regulates IgA selection and bacterial composition in the gut. *Science* **336**, 485–489 (2012).
53. T. Rollenske, S. Burkhalter, L. Muerner, S. von Gunten, J. Lukasiewicz, H. Wardemann, A. J. Macpherson, Parallelism of intestinal secretory IgA shapes functional microbial fitness. *Nature* **598**, 657–661 (2021).
54. J. Mirpuri, M. Raetz, C. R. Sturge, C. L. Wilhelm, A. Benson, R. C. Savani, L. V. Hooper, F. Yarovinsky, Proteobacteria-specific IgA regulates maturation of the intestinal microbiota. *Gut Microbes* **5**, 28–39 (2014).
55. P. E. Conrey, L. Denu, K. C. O'Boyle, I. Rozich, J. Green, J. Maslanka, J.-B. Lubin, T. Duranova, B. L. Haltzman, L. Gianchetti, D. A. Oldridge, N. De Luna, L. A. Vella, D. Allman, J. M. Spergel, C. Tanes, K. Bittinger, S. E. Henrickson, M. A. Silverman, IgA deficiency destabilizes homeostasis toward intestinal microbes and increases systemic immune dysregulation. *Sci. Immunol.* **8**, eade2335 (2023).
56. E. L. Kuan, S. Ivanov, E. A. Bridenbaugh, G. Victora, W. Wang, E. W. Childs, A. M. Platt, C. V. Jakubzick, R. J. Mason, A. A. Gashev, M. Nussenzweig, M. A. Swartz, M. L. Dustin, D. C. Zawieja, G. J. Randolph, Collecting lymphatic vessel permeability facilitates adipose tissue inflammation and distribution of antigen to lymph node-homing adipose tissue dendritic cells. *J. Immunol.* **194**, 5200–5210 (2015).
57. L. H. Jackson-Jones, P. Smith, J. R. Portman, M. S. Magalhaes, K. J. Mylonas, M. M. Vermeren, M. Nixon, B. E. P. Henderson, R. Dobie, S. Vermeren, L. Denby,

N. C. Henderson, D. J. Mole, C. Bénézech, Stromal cells covering omental fat-associated lymphoid clusters trigger formation of neutrophil aggregates to capture peritoneal contaminants. *Immunity* **52**, 700–715.e6 (2020).
58. I. Wernstedt Asterholm, C. Tao, T. S. Morley, Q. A. Wang, F. Delgado-Lopez, Z. V. Wang, P. E. Scherer, Adipocyte inflammation is essential for healthy adipose tissue expansion and remodeling. *Cell Metab.* **20**, 103–118 (2014).
59. C. Bénézech, N.-T. Luu, J. A. Walker, A. A. Kruglov, Y. Loo, K. Nakamura, Y. Zhang, S. Nayar, L. H. Jones, A. Flores-Langarica, A. McIntosh, J. Marshall, F. Barone, G. Besra, K. Miles, J. E. Allen, M. Gray, G. Kollias, A. F. Cunningham, D. R. Withers, K. M. Toellner, N. D. Jones, M. Veldhoen, S. A. Nedospasov, A. N. J. McKenzie, J. H. Caamaño, Inflammation-induced formation of fat-associated lymphoid clusters. *Nat. Immunol.* **16**, 819–828 (2015).
60. C. Perez-Shibayama, C. Gil-Cruz, H.-W. Cheng, L. Onder, A. Printz, U. Mörbe, M. Novkovic, C. Li, C. Lopez-Macias, M. B. Buechler, S. J. Turley, M. Mack, C. Soneson, M. D. Robinson, E. Scandella, J. Gommerman, B. Ludewig, Fibroblastic reticular cells initiate immune responses in visceral adipose tissues and secure peritoneal immunity. *Sci. Immunol.* **3**, eaar4539 (2018).
61. F. Raso, S. Liu, M. J. Simpson, G. M. Barton, C. T. Mayer, M. Acharya, J. R. Muppidi, A. Marshak-Rothstein, A. Reboldi, Antigen receptor signaling and cell death resistance controls intestinal humoral response zonation. *Immunity* **56**, 2373–2387.e8 (2023).
62. M. Nus, A. P. Sage, Y. Lu, L. Masters, B. Y. H. Lam, S. Newland, S. Weller, D. Tsiantoulas, J. Raffort, D. Marcus, A. Finigan, L. Kitt, N. Figg, R. Schirmbeck, M. Kneilling, G. S. H. Yeo, C. J. Binder, J. L. de la Pompa, Z. Mallat, Marginal zone B cells control the response of follicular helper T cells to a high-cholesterol diet. *Nat. Med.* **23**, 601–610 (2017).
63. L. F. Mager, R. Burkhard, N. Pett, N. C. A. Cooke, K. Brown, H. Ramay, S. Paik, J. Stagg, R. A. Groves, M. Gallo, I. A. Lewis, M. B. Geuking, K. D. McCoy, Microbiome-derived inosine modulates response to checkpoint inhibitor immunotherapy. *Science* **369**, 1481–1489 (2020).
64. H. Nishimura, N. Minato, T. Nakano, T. Honjo, Immunological studies on PD-1 deficient mice: Implication of PD-1 as a negative regulator for B cell responses. *Int. Immunol.* **10**, 1563–1572 (1998).
65. A. Wiedemann, M. Lettau, I. Wirries, A. Jungmann, A. Salhab, G. Gasparoni, H. E. Mei, C. Perka, J. Walter, A. Radbruch, A. C. Lino, T. Dörner, Human IgA-expressing bone marrow plasma cells characteristically upregulate programmed cell death protein-1 upon B cell receptor stimulation. *Front. Immunol.* **11**, 628923 (2021).
66. S. Vergani, K. G. Muleta, C. Da Silva, A. Doyle, T. A. Kristiansen, S. Sodini, N. Krausse, G. Montano, K. Kotarsky, J. Nakawesi, H. Åkerstrand, S. Vanhee, S. L. Gupta, D. Bryder, W. W. Agace, K. Lahl, J. Yuan, A self-sustaining layer of early-life-origin B cells drives steady-state IgA responses in the adult gut. *Immunity* **55**, 1829–1842.e6 (2022).
67. D. Sterlin, G. Gorochov, When therapeutic IgA antibodies might come of age. *Pharmacology* **106**, 9–19 (2021).
68. J. J. Faith, P. P. Ahern, V. K. Ridaura, J. Cheng, J. I. Gordon, Identifying gut microbe-host phenotype relationships using combinatorial communities in gnotobiotic mice. *Sci. Transl. Med.* **6**, 220ra11 (2014).
69. H.-E. Ho, L. Radigan, G. Bongers, A. El-Shamy, C. Cunningham-Rundles, Circulating bioactive bacterial DNA is associated with immune activation and complications in common variable immunodeficiency. *JCI Insight* **6**, e144777 (2021).
70. A. Aghamohammadi, T. Cheraghi, M. Gharagozlou, M. Movahedi, N. Rezaei, M. Yeganeh, N. Parvaneh, H. Abolhassani, Z. Pourpak, M. Moin, IgA deficiency: Correlation between clinical and immunological phenotypes. *J. Clin. Immunol.* **29**, 130–136 (2009).
71. D. E. Briles, J. Latham Claflin, K. Schroer, C. Forman, Mouse IgG3 antibodies are highly protective against infection with Streptococcus pneumoniae. *Nature* **294**, 88–90 (1981).
72. G. R. Siber, P. H. Schur, A. C. Aisenberg, S. A. Weitzman, G. Schiffman, Correlation between serum IgG-2 concentrations and the antibody response to bacterial polysaccharide antigens. *N. Engl. J. Med.* **303**, 178–182 (1980).
73. H. Sokol, C. Lay, P. Seksik, G. W. Tannock, Analysis of bacterial bowel communities of IBD patients: What has it revealed? *Inflamm Bowel Dis.* **14**, 858–867 (2008).
74. A. Chudnovskiy, A. Mortha, V. Kana, A. Kennard, J. D. Ramirez, A. Rahman, R. Remark, I. Mogno, R. Ng, S. Gnjatic, E.-A. D. Amir, A. Solovyov, B. Greenbaum, J. Clemente, J. Faith, Y. Belkaid, M. E. Grigg, M. Merad, Host-protozoan interactions protect from mucosal infections through activation of the inflammasome. *Cell* **167**, 444–456.e14 (2016).
75. M. R. Hepworth, L. A. Monticelli, T. C. Fung, C. G. K. Ziegler, S. Grunberg, R. Sinha, A. R. Mantegazza, H.-L. Ma, A. Crawford, J. M. Angelosanto, E. J. Wherry, P. A. Koni, F. D. Bushman, C. O. Elson, G. Eberl, D. Artis, G. F. Sonnenberg, Innate lymphoid cells regulate $CD4^+$ T-cell responses to intestinal commensal bacteria. *Nature* **498**, 113–117 (2013).
76. M. D. Robinson, A. Oshlack, A scaling normalization method for differential expression analysis of RNA-seq data. *Genome Biol.* **11**, R25 (2010).
77. I. Wanigasuriya, Q. Gouil, S. A. Kinkel, A. Tapia del Fierro, T. Beck, E. A. Roper, K. Breslin, J. Stringer, K. Hutt, H. J. Lee, A. Keniry, M. E. Ritchie, M. E. Blewitt, Smchd1 is a maternal effect gene required for genomic imprinting. *eLife* **9**, e55529 (2020).
78. C. W. Law, Y. Chen, W. Shi, G. K. Smyth, voom: Precision weights unlock linear model analysis tools for RNA-seq read counts. *Genome Biol.* **15**, R29 (2014).
79. S. Durinck, Y. Moreau, A. Kasprzyk, S. Davis, B. De Moor, A. Brazma, W. Huber, BioMart and Bioconductor: A powerful link between biological databases and microarray data analysis. *Bioinformatics* **21**, 3439–3440 (2005).
80. S. Durinck, P. T. Spellman, E. Birney, W. Huber, Mapping identifiers for the integration of genomic datasets with the R/Bioconductor package biomaRt. *Nat. Protoc.* **4**, 1184–1191 (2009).
81. E. Bolyen, J. R. Rideout, M. R. Dillon, N. A. Bokulich, C. C. Abnet, G. A. Al-Ghalith, H. Alexander, E. J. Alm, M. Arumugam, F. Asnicar, Y. Bai, J. E. Bisanz, K. Bittinger, A. Brejnrod, C. J. Brislawn, C. T. Brown, B. J. Callahan, A. M. Caraballo-Rodríguez, J. Chase, E. K. Cope, R. Da Silva, C. Diener, P. C. Dorrestein, G. M. Douglas, D. M. Durall, C. Duvallet, C. F. Edwardson, M. Ernst, M. Estaki, J. Fouquier, J. M. Gauglitz, S. M. Gibbons, D. L. Gibson, A. Gonzalez, K. Gorlick, J. Guo, B. Hillmann, S. Holmes, H. Holste, C. Huttenhower, G. A. Huttley, S. Janssen, A. K. Jarmusch, L. Jiang, B. D. Kaehler, K. B. Kang, C. R. Keefe, P. Keim, S. T. Kelley, D. Knights, I. Koester, T. Kosciolek, J. Kreps, M. G. I. Langille, J. Lee, R. Ley, Y.-X. Liu, E. Loftfield, C. Lozupone, M. Maher, C. Marotz, B. D. Martin, D. McDonald, L. J. McIver, A. V. Melnik, J. L. Metcalf, S. C. Morgan, J. T. Morton, A. T. Naimey, J. A. Navas-Molina, L. F. Nothias, S. B. Orchanian, T. Pearson, S. L. Peoples, D. Petras, M. L. Preuss, E. Pruesse, L. B. Rasmussen, A. Rivers, M. S. Robeson, P. Rosenthal, N. Segata, M. Shaffer, A. Shiffer, R. Sinha, S. J. Song, J. R. Spear, A. D. Swafford, L. R. Thompson, P. J. Torres, P. Trinh, A. Tripathi, P. J. Turnbaugh, S. Ul-Hasan, J. J. J. van der Hooft, F. Vargas, Y. Vázquez-Baeza, E. Vogtmann, M. von Hippel, W. Walters, Y. Wan, M. Wang, J. Warren, K. C. Weber, C. H. D. Williamson, A. D. Willis, Z. Z. Xu, J. R. Zaneveld, Y. Zhang, Q. Zhu, R. Knight, J. G. Caporaso, Reproducible, interactive, scalable and extensible microbiome data science using QIIME 2. *Nat. Biotechnol.* **37**, 852–857 (2019).
82. B. J. Callahan, P. J. McMurdie, M. J. Rosen, A. W. Han, A. J. A. Johnson, S. P. Holmes, DADA2: High-resolution sample inference from Illumina amplicon data. *Nat. Methods* **13**, 581–583 (2016).
83. D. McDonald, M. N. Price, J. Goodrich, E. P. Nawrocki, T. Z. DeSantis, A. Probst, G. L. Andersen, R. Knight, P. Hugenholtz, An improved Greengenes taxonomy with explicit ranks for ecological and evolutionary analyses of bacteria and archaea. *ISME J.* **6**, 610–618 (2012).
84. G. M. Douglas, V. J. Maffei, J. R. Zaneveld, S. N. Yurgel, J. R. Brown, C. M. Taylor, C. Huttenhower, M. G. I. Langille, PICRUSt2 for prediction of metagenome functions. *Nat. Biotechnol.* **38**, 685–688 (2020).
85. C. Lozupone, R. Knight, UniFrac: A new phylogenetic method for comparing microbial communities. *Appl. Environ. Microbiol.* **71**, 8228–8235 (2005).
86. A. Subramanian, P. Tamayo, V. K. Mootha, S. Mukherjee, B. L. Ebert, M. A. Gillette, A. Paulovich, S. L. Pomeroy, T. R. Golub, E. S. Lander, J. P. Mesirov, Gene set enrichment analysis: A knowledge-based approach for interpreting genome-wide expression profiles. *Proc. Natl. Acad. Sci. U.S.A.* **102**, 15545–15550 (2005).

Acknowledgments

Funding: This work was supported by US National Institutes of Health grants P01 AI61093 to C.C.-R. and A.C., R01 DK123749 to A.C., J.J.F., and S.M., R01 DK114038 to J.C.C., K23 AI137183 to P.J.M., and R21AI168718 to E.K.G.; Crohn's and Colitis Foundation CDA 877970 to E.K.G.; Ministerio de Ciencia, Innovación y Universidades grant RTI2018-093894-B-I00 and European Advanced grant ERC-2011-ADG-20110310 to A.C.; and the Institute of Health Carlos III-Miguel Servet research program to G.M. **Author contributions:** Conceptualization: A.C., C.G., and E.K.G. Methodology: C.G., E.K.G., P.J.M., G.M., G.J.B., A.M.N., M.G.P., M.M.G., R.D.-C., M.S.-F., J.C.C., J.J.F., C.C.-R., and A.C. Investigation: C.G., E.K.G., D.B.M., G.J.B., H.M., G.M., L.T., M.St., M.So., P.C.-H., M.P., S.T.V., L.R., R.T.-P., A.M.N., M.G.P., M.M.G., and R.D.-C. Visualization: C.G., E.K.G., D.B.M., G.M., G.J.B., and L.T. Funding acquisition: A.C., C.C.R., J.J.F., S.M., G.M., and P.J.M. Project administration: A.C. and C.G. Supervision: A.C., C.G., and E.K.G. Writing—original draft: A.C., C.G., and E.K.G. Writing—review and editing: A.C., E.K.G., M.G., J.J.F., J.C.C., C.G., C.C.-R., D.B.M., P.C.-H., M.So., A.M.N., M.G.P., M.M.G., R.D.-C., and S.M. **Competing interests:** The authors declare that they have no competing interests. **Data and materials availability:** All data needed to evaluate the conclusions in the paper are present in the paper and/or the Supplementary Materials. RNA-seq sequence data files (fastq) are stored in the public SRA under project number PRJNA725246, whereas 16*S* sequence data files (fastq) are stored in the public SRA under project number PRJNA722766.

Submitted 28 February 2024
Accepted 13 January 2025
Published 12 February 2025
10.1126/sciadv.ado9455